Title:
Cytostatic hypothermia and its impact on glioblastoma and survival

Authors:
Syed Faaiz Enam[1*], Cem Y. Kilic[1,4], Jianxi Huang[1,4], Brian J. Kang[1], Reed Chen[1], Connor S. Tribble[1], Martha I. Betancur[1], Ekaterina Ilich[1], Stephanie J. Blocker[2], Steven Owen[3], Johnathan G. Lyon[1], Ravi V. Bellamkonda[1*]

Affiliations:
[1]Department of Biomedical Engineering, Pratt School of Engineering, Duke University, Durham, NC 27705
[2]Department of Radiology, Center for In Vivo Microscopy, Duke University, Durham, NC 27705
[3]Bio-medical Machine Shop, Pratt School of Engineering, Duke University, Durham, NC 27705
[4]these authors contributed equally to the manuscript

[*]co-corresponding authors:
Syed Faaiz Enam: faaiz.enam@duke.edu
Ravi V. Bellamkonda: ravi@duke.edu

Abstract:
Novel therapeutic approaches are needed for patients with recurrent glioblastoma (GBM) who otherwise have limited options. Hypothermia has been used to cryo-ablate tumor locally, but this is ineffective against infiltrative cells as it damages healthy tissue too. Here we developed and deployed local 'cytostatic' hypothermia to stunt GBM growth. We first investigated three grades of hypothermia *in vitro* and identified a cytostatic window of 20–25°C. We also determined that 18 h/d of cytostatic hypothermia can be sufficient to prevent growth. Cytostatic hypothermia resulted in cell cycle arrest, reduced metabolite production and consumption, and reduced inflammatory cytokine synthesis. We designed a device to deliver local cytostatic hypothermia *in vivo* in two rodent models of GBM: utilizing the rat F98 and the human U-87 MG lines. Local hypothermia more than doubled the median survival of F98 bearing rats from 3.9 weeks to 9.7 weeks. Two rats survived through 12 weeks. No loss of U-87 MG bearing rats was observed during their study period of 9 weeks. Additionally, we demonstrated that cytostatic hypothermia is synergistic with chemotherapy *in vitro*. Interestingly, we also demonstrate that CAR T immunotherapy can function with cytostatic hypothermia. Unlike modern targeted therapeutics, cytostatic hypothermia affects multiple cellular processes simultaneously. Thus, irrespective of the host species (e.g., rodent vs. human), it could slow tumor progression and the evolution of resistance. Our studies show that this approach enhances progression-free survival without chemical interventions. However, it may also provide time and opportunities to use standard concomitant, adjuvant, and novel cytotoxic treatments. Therefore, local cytostatic hypothermia could be a critical addition to the limited options patients with GBM have.

Keywords:
hypothermia, glioblastoma, cancer, cytostatic, local, focal, cooling

Acknowledgements:
We are grateful to: Dr. Nalini Mehta and Sheridan Carroll for generating CAR T cells; Steven 'Joe' Owen at the Pratt Bio-medical Machine Shop for his assistance in designing and fabricating hypothermia devices; the Center for In Vivo Microscopy at Duke University for MR imaging; the staff (Kaylee Lynn, Bridget Pickle, Jesse DeGraff, and Fernando Orozco) and veterinarians (Drs. Felicitas Smith and Clay Rouse) at the Duke Vivarium for their assistance in setting up and maintaining animal experiments; Dr. Syed A. Enam for his neurosurgical insights; and Edward Mallon for his advice on setting up a temperature recording system.

1. INTRODUCTION

Despite standard-of-care treatment, patients with glioblastoma (GBM) have a poor median survival of 15–18 months. At best, ~7% survive 5 years after diagnosis[1,2]. This is due to the ineffectiveness of current therapies, resulting in nearly all GBMs recurring. Interestingly more than 80% of recurrences are local[3–5], which provides a role for local therapies. Unfortunately, due to the traumatic effects of treatment, only 20–30% of the recurrences can be resected before recurring once more[6].

The ineffectiveness of current GBM therapies necessitates novel domains of therapeutics, such as manipulating physical phenomena like electric fields, topographical guidance, and temperature. For example, tumor-treating electric fields can disrupt mitosis and have demonstrated a mild effect on overall survival[7,8]. Topological cues of aligned nanofibers can induce directional migration of GBM to a cytotoxic sink[9], and this strategy recently received FDA breakthrough status. In fact, directional GBM migration may also be induced by applying electric fields[10]. Both hyper- and hypo-thermia have been used to successfully kill tumor cells[11,12]. Thus, approaches that leverage physics may expand the repertoire of options available to GBM patients.

Hypothermia as a cancer therapy remains relatively under-explored and can be divided into two forms: cryogenic (freezing) and non-cryogenic hypothermia. Currently, our only hypothermia-driven approach against cancer is cryosurgery[13]. In the 1940s, neurosurgeon Dr. Temple Fay first applied whole-body hypothermia to limit tumor growth, but this proved to be hazardous and infeasible[14]. He then attempted locally freezing tumor in one glioma patient with a cryoprobe tethered to a 'beer cooler'[14]. However, the degree, duration, intermittency, and follow-up of this case is not detailed, possibly due to hypothermia falling out of favor after it was misused during World War II[15]. Subsequently, cryogenic freezing of brain tumors was repeated and cryosurgery was born[12,16]. However, subzero temperatures indiscriminately ablate diseased and healthy tissue[13,17]. Thus, cryogenic freezing offers little advantage over current GBM therapies.

Alternatively, the healthy brain is resilient to severe, but non-cryogenic hypothermia[14,18,19]. Additionally, temperatures of 32–35°C may be neuroprotective after injury[20]. This moderate hypothermia reduces cell metabolism, oxygen and glucose consumption, edema, excitotoxicity, and free-radical formation[20]. In epilepsy, novel cortical cooling devices can halt seizures in primates[19,21] and intraoperatively in patients[22]. Thus, non-cryogenic hypothermia could have therapeutic utility without significant cortical damage.

In this study, we propose non-ablative hypothermia for brain tumors, which we term 'cytostatic hypothermia', to halt tumor growth and leave minimal damage. We first identified a window of temperatures that halts cell division. This is corroborated by recent *in vitro* studies[23–27] that confirm a 1959 finding suggesting hypothermia reduces cell proliferation[14]. We investigated the effects of the degree and duration of hypothermia on the growth and metabolism of multiple human GBM lines *in vitro*. We suggest that by leveraging a *physical* phenomenon (hypothermia), multiple cellular pathways are modulated simultaneously, and these effects may thus not be species-specific (i.e., may be translatable to humans). Next, capitalizing on the brain's resilience to hypothermia, we modelled and designed a device to locally deliver cytostatic hypothermia *in vivo*. Then we tested this device in two models of GBM in rats. Finally, we explored the concomitant and adjuvant potential of hypothermia *in vitro* with chemotherapy and chimeric antigen receptor T cell (CAR T) immunotherapy. Based on our findings, local cytostatic hypothermia could be a much-needed option for patients who would otherwise succumb to GBM.

2. RESULTS

a. *In vitro* tumor growth and viability are influenced by the degree and duration of hypothermia.

To investigate how different degrees of hypothermia affect cell growth rates, we cultured three human GBM cell lines and one rat GBM line at 20, 25, 30 and 37°C. Growth was assessed daily through a custom live-cell imaging and analysis method we developed (Fig. 1a). It used contrast and edge detection with optimized thresholds to identify tumor coverage as a proxy for growth in a 2D well. All cell lines grew at 37°C (Supplementary Fig. 1a) and became fully confluent within 3–5 days (Fig. 1b). Reducing the temperature to 30°C reduced growth rates such that a significant difference in cell coverage was observed out to 12 days in three lines. Furthermore, three human GBM lines all showed no growth at 25°C (Fig. 1b, Supplementary Fig. 1b). Interestingly, while F98 (rat GBM) did have significantly reduced coverage at 12 days under 25°C, it required 20°C to halt growth (Fig. 1b, Supplementary Fig. 1c).

To explore the minimum daily duration of cooling required to maintain cytostasis, we cycled the plates between a 37°C and 25°C incubator for a pre-defined number of hours per day (h/d). The temperature change of the media had a rapid phase followed by a slow phase, reaching the desired temperature within 30–60 minutes (Supplementary Fig. 2a). The growth rate of all cell lines was significantly reduced with as little as 16 h/d of 25°C hypothermia compared to 37°C (Supplementary Fig. 2b). The application of 20 h/d of 20°C hypothermia on F98 also reduced its growth rate compared to 25°C (Supplementary Fig. 2c). With the addition of a 4-day 25°C pretreatment period, growth rates were significantly affected (Fig. 1c) such that T98G and LN-229 demonstrated equivalent well coverage on day 12 with day 4 after 18 h/d hypothermia (Fig. 1c).

To assess cell viability after prolonged hypothermia, at predetermined timepoints (7, 14, 21, and 28 d) we used an end-point Live-Dead assay (Fig. 1d) and, in a separate assay, observed growth after returning the cells to 37°C (Fig. 1e). All three human GBM lines demonstrated a reduction in the Live:Dead ratio at 25°C with T98G being the most affected (Fig. 1d). Similarly, growth of human GBM lines lagged after prolonged 25°C exposure with significantly reduced cell coverage 7 days after returning to 37°C (Fig. 1e).

The custom imaging assay also facilitated assessment of morphological features of circularity and average size. Compared to cell circularity after overnight incubation at 37°C (day 0), hypothermia significantly increased U-87 MG and LN-229 circularity (Supplementary Fig. 2d) while T98G remained unaffected. While F98 circularity significantly decreased with hypothermia over time, it displayed significantly greater circularity under 20°C compared to 25°C. Similarly, average cell size of U-87 MG and T98G were significantly reduced with prolonged hypothermia (Supplementary Fig. 2e). F98 demonstrated an increase in the average cell size under 25°C, but this was abrogated under its cytostatic temperature of 20°C (Supplementary Fig. 2e).

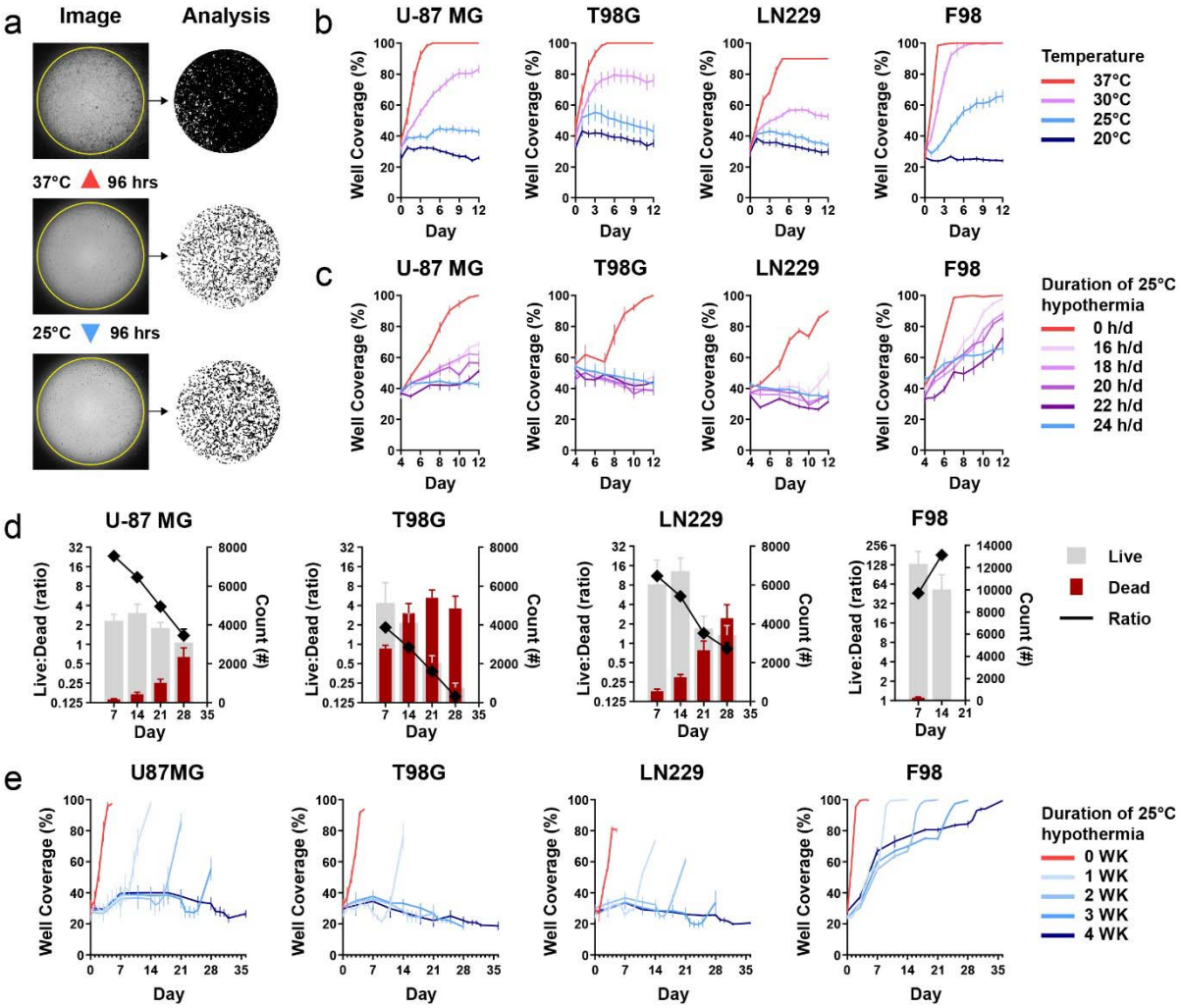

Figure 1: Effect of continuous and intermittent cytostatic hypothermia on GBM cell lines *in vitro*. (a) Custom imaging and tumor well coverage analysis assay with photos (left) and resulting masks (right). Cells were grown overnight at 37°C and then imaged and grown in 96-well plates under either normo- or hypo- thermia. A custom ImageJ macro identified tumor from background and quantified confluence. On the masks, black represents cells and white represents the well. **(b)** GBM growth curves via percent of well coverage at 37, 30, 25, and 20°C; two-way ANOVA with Dunnett's multiple comparisons test demonstrated $p < 0.0001$ at day 12 between all hypothermia conditions and 37°C across all lines, except for F98 at 30°C (non-significant). **(c)** GBM growth rates under intermittent 25°C hypothermia after 25°C pre-treatment. Cells were plated and grown overnight at 37°C, followed by 4 days under 25°C hypothermia (pre-treatment). Beginning day 4, cells were transferred between 37°C and 25°C incubators for varying hours per day (h/d); two-way ANOVA with Dunnett's multiple comparisons test demonstrated $p < 0.0001$ at day 12 between all duration and 0 h/d across all lines, except for F98 at 16 h/d ($p = 0.0013$). **(d)** Live/Dead assay of GBM lines over time at 25°C. Groups of the same line were stained with fluorescent microscopy-based live/dead dyes. A custom ImageJ macro counted the number of living (grey) and dead cells (maroon) plotted on the right y-axis. A ratio of live:dead was calculated and plotted on the left y-axis. **(e)** Cell viability imaging assay. Cells were grown at 25°C for 0, 1, 2, 3, and 4 weeks. At respective time points, the cells were moved to 37°C and imaged daily.

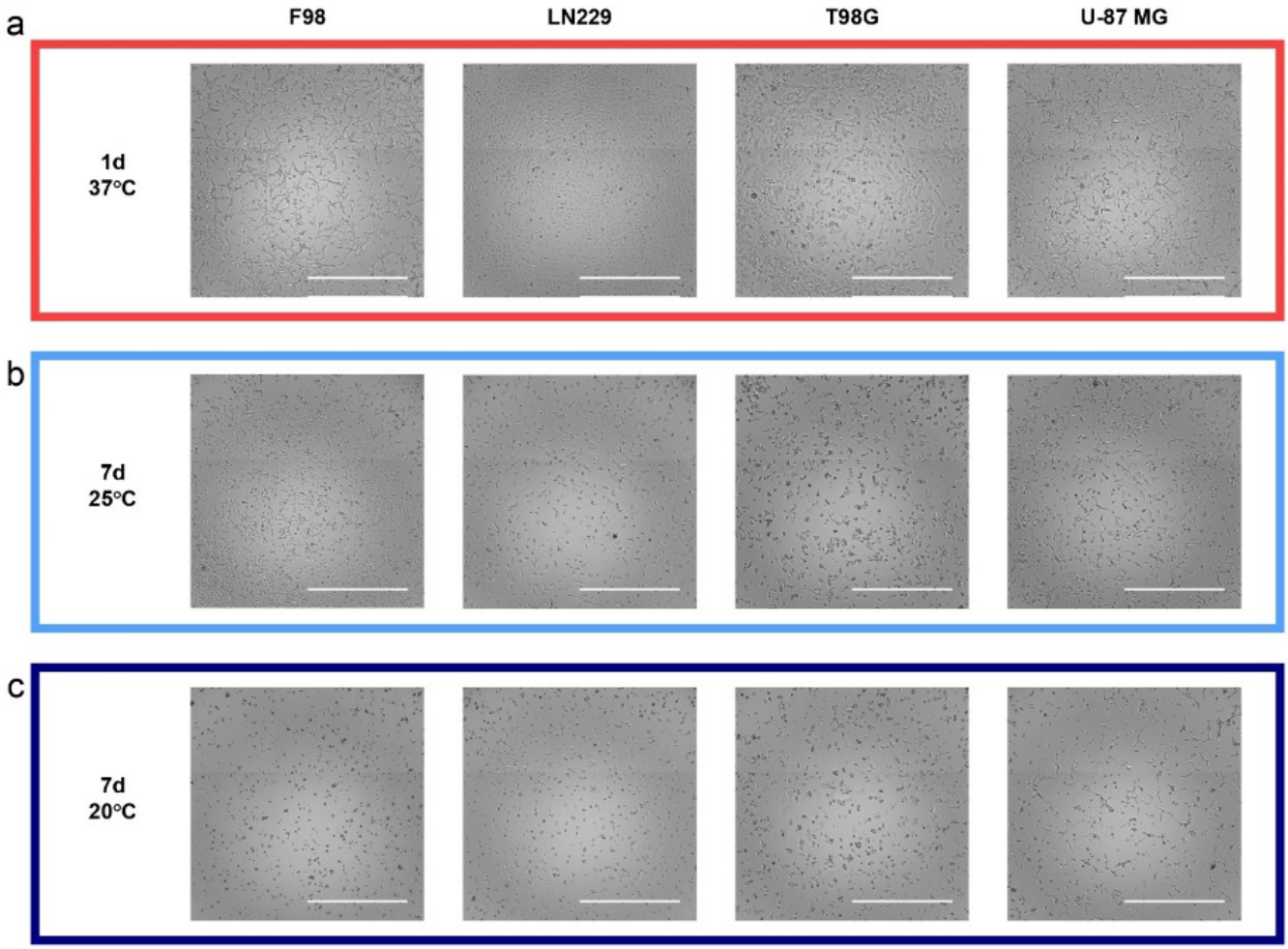

Supplementary Figure 1: Brightfield images of GBM lines under different temperature conditions. All cells received overnight incubation at 37°C and then were either left at 37°C or transferred to 25°C or 20°C**. (a)** Images of cells after 1 day at 37°C. **(b)** Images of cells after 7 days at 25°C. **(c)** Images of cells after 7 days at 20°C.

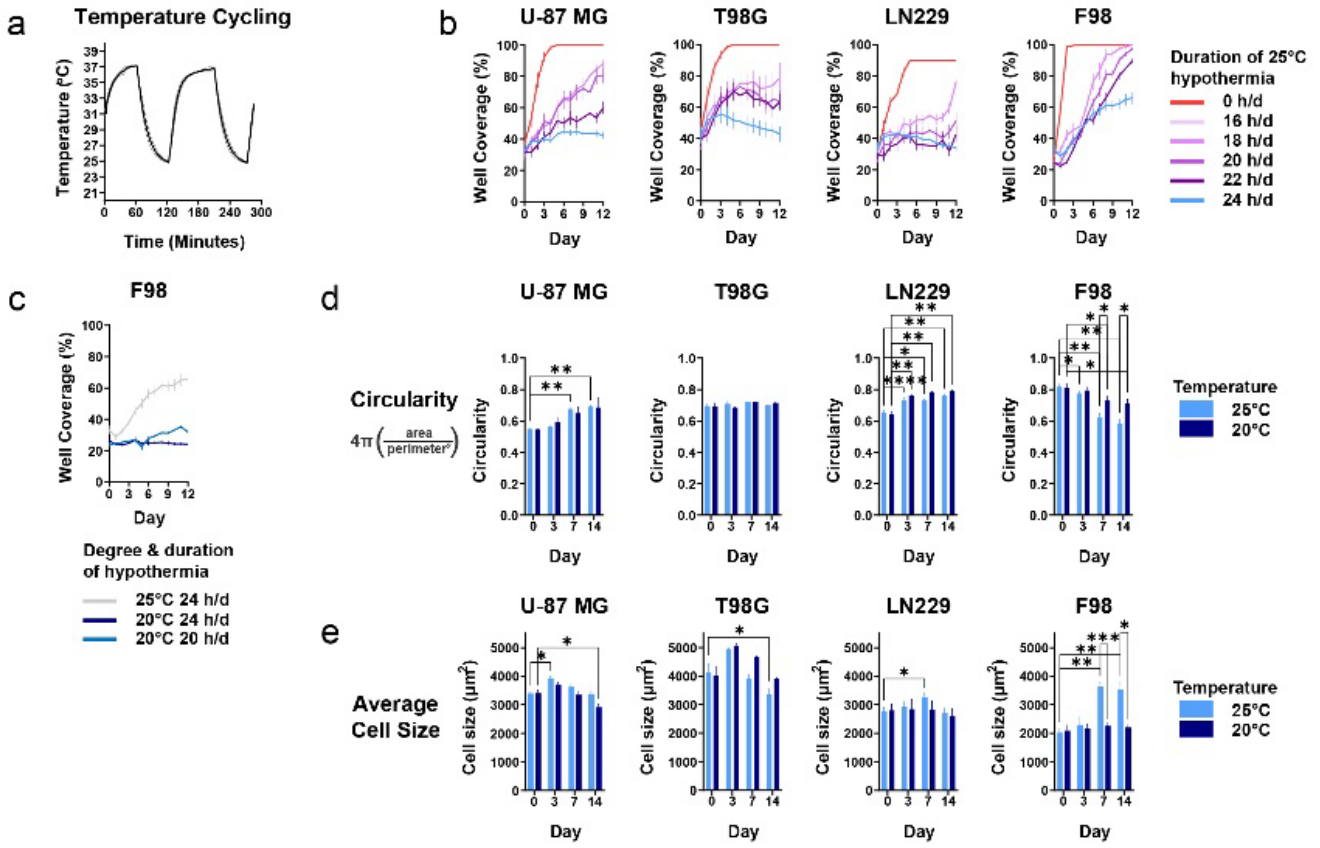

Supplementary Figure 2: Effect of intermittent hypothermia on cell growth and continuous hypothermia on cell morphology. (a) Plot demonstrating the change of media temperature when a microplate is transferred between 37°C and 25°C cell incubators. Thermistors were attached on the bottom of a central well and lateral well. Resistance was measured with a voltage-divider circuit and Arduino and converted to temperature with a script. **(b)** GBM growth rates under intermittent 25°C hypothermia without 25°C pre-treatment. Plates were transferred between 37°C and 25°C incubator for varying hours/day (h/d). **(c)** F98 growth rate under continuous 25°C or 20°C hypothermia or 20 h/d intermittent 20°C hypothermia with 4 days of 20°C pretreatment. **(d) and (e)** Average tumor cell circularity and average size under hypothermia. Circularity and average size were determined through ImageJ. Two-way ANOVAs were conducted with Dunnet's multiple comparison tests post-hoc (*p<0.05, **p<0.01, ***p<0.001, ****p<0.0001).

b. Hypothermia arrests the cell cycle and reduces metabolism and cytokine synthesis.

To further investigate the effects of cytostatic hypothermia, we assayed cell cycle, ATP levels, metabolite production/consumption, and cytokine production under hypothermia. Cells grown for 3 days at 37°C were predominantly in the G1 phase of the cell cycle (Fig. 2a). The application of 3 or 7 days of 25°C, induced a significant reduction in both the G1- and S-phases along with an increase in the G2-phase across all cell lines (Fig. 2a). Next, we quantified intracellular ATP to investigate whether ATP production and consumption ceased. Interestingly, intracellular ATP was significantly reduced in T98G but significantly greater in the remaining 3 lines under 25°C hypothermia (Fig. 2b). Next, we assayed media glucose, lactate, glutamate, and glutamine at 0, 3, 7, and 14 days at 20, 25, 30, and 37°C (Fig. 2c and Supplementary Fig. 3). To account for cell growth under non-cytostatic conditions, the data was normalized to tumor-cell occupied surface area using our imaging assay (Fig. 2c). Results demonstrated that metabolite production and consumption are significantly reduced with any degree of hypothermia. However, F98 glutamate production was not significantly different at day 3 (Fig. 2c) but remained low under 20°C (Supplementary Fig. 3d). Similarly, expression of inflammatory cytokines IL-6 and IL-8 from human GBM lines were significantly lower after 6 or 10 days of hypothermia (Fig. 2d). Interestingly, a mild but significant increase of both cytokines was observed after the first 3 days of 25°C from T98G, but it

subsided by day 6. We did not detect expression of anti-inflammatory cytokines IL-4, IL-10, or the inflammatory cytokine IFNγ under any condition.

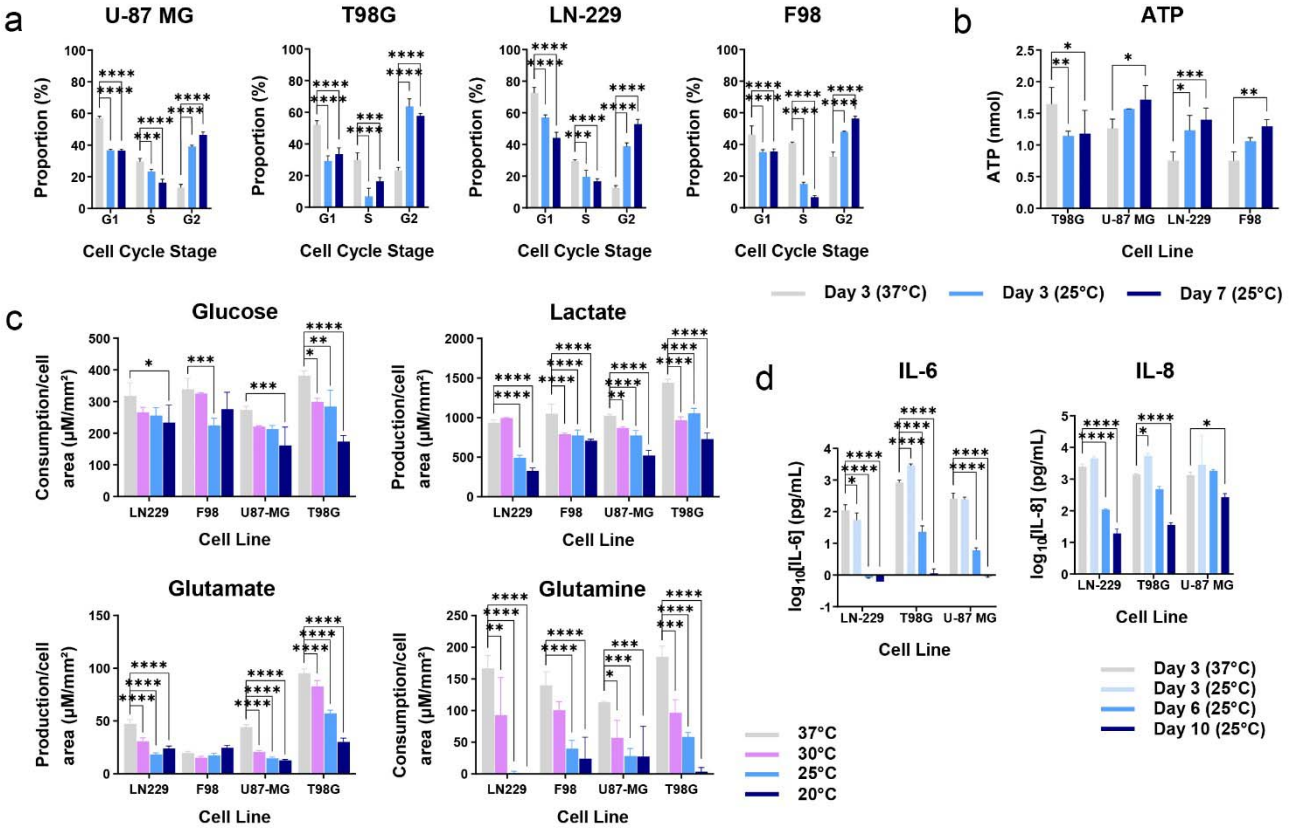

Figure 2: Effects of hypothermia on tumor cell cycle, metabolism, and cytokine synthesis. (a) Percentage of cells in each stage of the cell cycle after either 3 days of 37°C, 3 days of 25°C, or 7 days of 25°C. **(b)** Amount of intracellular ATP from the tumor cell lines when grown for 3 days at 37°C, 3 days at 25°C, or 7 days at 25°C. **(c)** Metabolite production or consumption per cell surface area across cell lines and temperatures after either 3 days of 37°C or 3 days of hypothermia (30°C, 25°C, 20°C). **(d)** Concentration of cytokines (IL-6 and IL-8) collected in the media at different time points and temperatures. All studies used two-way ANOVAs with post-hoc Dunnett's multiple comparison test (*p<0.05, **p<0.01, ***p<0.001, ****p<0.0001).

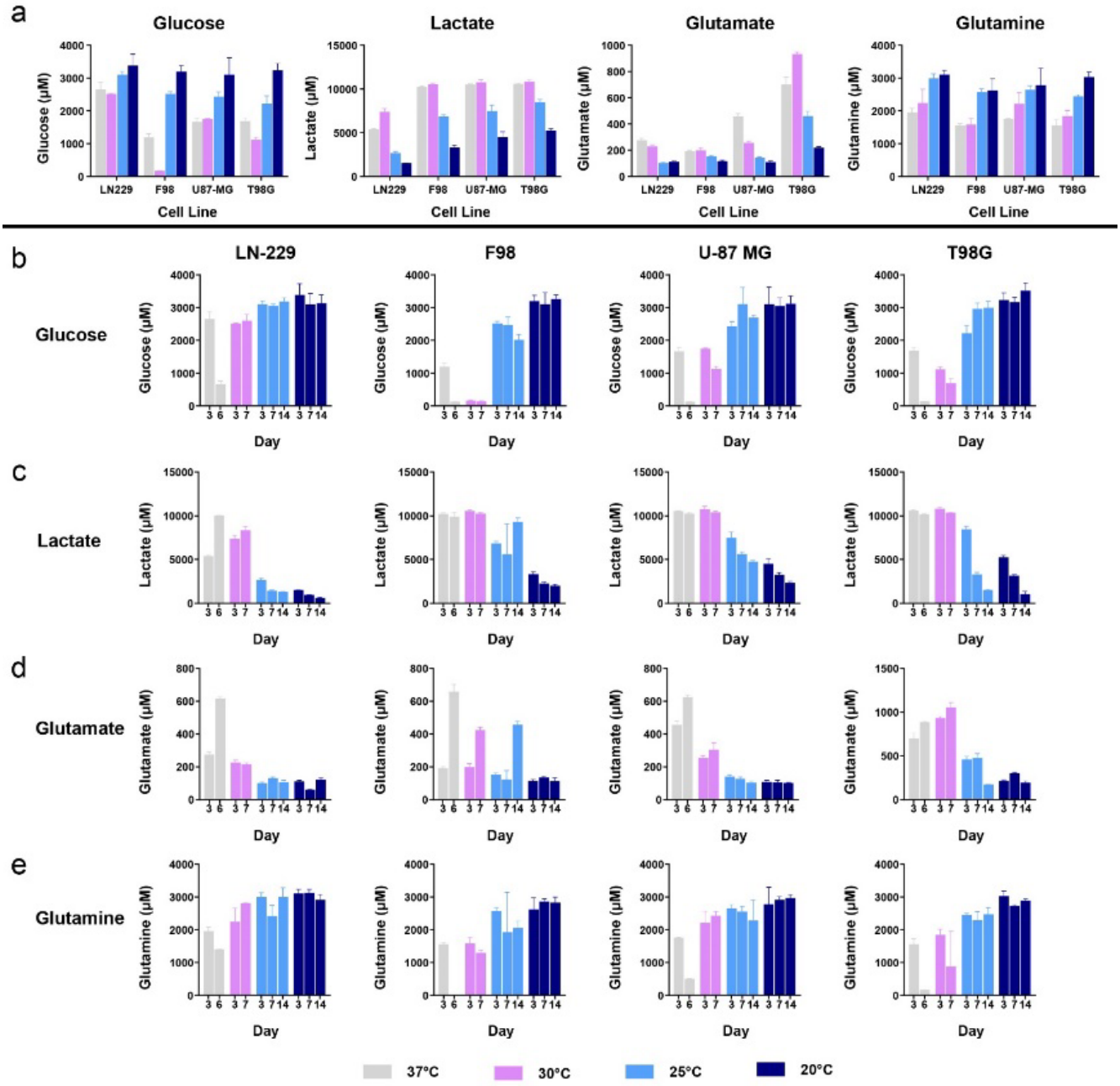

Supplementary Figure 3: Metabolite production and consumption under hypothermia. (a) Metabolite levels in media after 3 days at 37°C or 3 days at hypothermic temperatures (30, 25, or 20°C). **(b)** Glucose levels in media at 3, 7, and 14 days at different temperatures. **(c)** Lactate levels in media at 3, 7, and 14 days at different temperatures. **(d)** Glutamate levels in media at 3, 7, and 14 days at different temperatures. **(e)** Glutamine levels in media at 3, 7, and 14 days at different temperatures.

c. Local hypothermia can be delivered *in vivo* and reduces GBM tumor growth.

Given that hypothermia of 20–25°C halted cell division *in vitro* (Fig. 1a) we conceived a method to deliver hypothermia *in vivo* and assessed its effect on tumor growth. Using a computational finite-element method we modeled local intracranial hypothermia incorporating parameters from prior studies (Supplementary Table 1), Pennes' bio-heat equations, temperature-dependent blood perfusion, and a previously modeled rat brain[28] (Fig. 3a

and Supplementary Fig. 4a). A single 1-mm wide gold probe was modeled invaginating into the brain with a spherical tumor (1 and 1.5-mm radius) cooled via a Peltier plate pulling 125 mW of heat (Fig. 3b and Supplementary Fig. 4b). The simulation suggested that a probe at ~12°C could reduce the temperature of a 2-mm diameter tumor to <25°C (Fig. 3b). Cooling was greater across the x-axis (of a coronal plane) than down the z-axis but reached >35°C within 4 mm beyond the tumor (Fig. 3c, left). The extent of tumor perfusion (ranging from 0.73 to 3.96 times brain perfusion) had a small effect on cooling a modeled 3-mm tumor (Fig. 3c, middle). To achieve hypothermia in a 3-mm tumor, 125mW of heat pulled was sufficient to maintain 25°C hypothermia (Fig. 3c, right). Simulating a 150mW pull resulted in the probe reaching <0°C although the tissue was at 15°C within 0.5 mm from the probe (Fig 3c, right). A time-dependent study using the models suggested that pulling 100-125mW can bring the maximum tumor temperature to its target within 1–2 minutes (Supplementary Fig. 4c).

Next, we constructed a hypothermia device that consists of a removable 'Cooler' and an implantable 'Interface' (Fig. 3d and Supplementary Fig. 5). The Cooler uses an electrically powered thermoelectric (Peltier) plate secured between a copper plate embedded in a polycarbonate base and an aluminum heatsink with thermal paste (Fig. 3e). A fan, secured above, enhances convective heat transfer. The Interface attaches to the skull, has an intratumoral gold needle soldered to a second copper element, and a thermistor wired to insulated brass screws (Supplementary Fig. 5h and i). The copper parts make contact to transfer heat from the Interface to the Cooler (Supplementary Fig. 5l). This Cooler is powered through an external power supply. Temperature is measured by the thermistor connected to a voltage-divider circuit, Arduino, and a computer (Supplementary Fig. 6).

After inoculation with F98 tumor cells, tumor-take was confirmed in all rats via MRI at 1 week, and the Interface was implanted on the subsequent day (demonstrated in Supplementary Fig. 7a and b) followed by attachment of the Cooler. A custom cage setup was developed to enable free movement of the rats (Supplementary Fig. 7c–e). Once switched on, the device was able to reduce local temperature to 25°C, measured 1 mm from the intratumoral cooling probe surface (Fig. 3f). Devices did not consistently reach 20°C due to inefficiencies of our heat-exchange mechanism. Interfaces embedded with an MRI-compatible thermistor enabled tumor growth assessment via MRI (Fig. 3g). MRI image analysis revealed a significant difference in tumor volume growth for tumors at 1 week under hypothermia (device on) versus tumors at normothermia (device off) (Fig. 3h). Due to high failure rates of the MRI-compatible thermistor, subsequent studies used an MRI-incompatible thermistor with tighter tolerance and greater reliability.

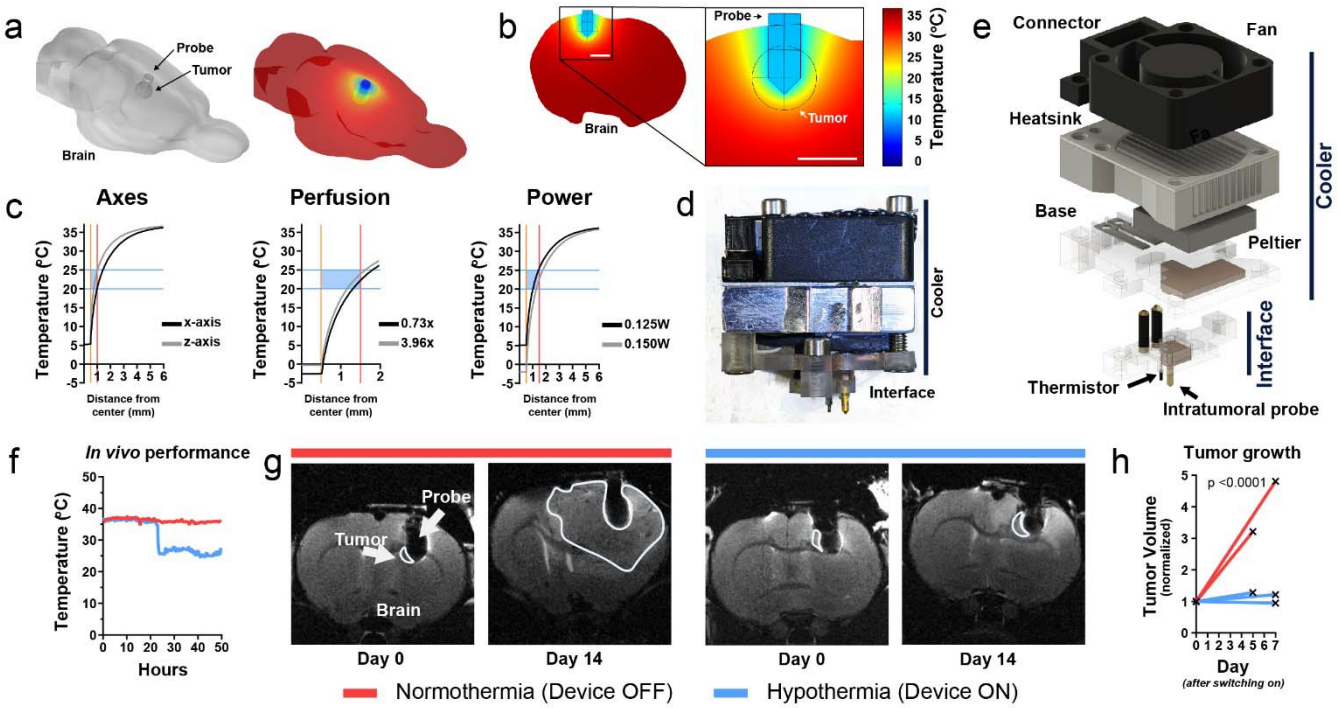

Figure 3: Finite-element analysis and device development for local cytostatic hypothermia delivery. (a) Left: 3D model of rat brain with a probe and subcortical spherical tumor. Right: finite-element simulation of temperature on the brain surface. **(b)** Slice and magnified inset from finite-element model of rat brain with local hypothermia. A 1-mm width probe in a 2-mm diameter tumor cooled to 12°C enabled tumor periphery to reach 25°C. **(c)** Finite-element analysis of hypothermia varying parameters. Center of tumor and probe lie at x=0. Gold bar indicates surface of gold cooling probe. Red bar indicates surface of tumor. Blue bars and box show cytostatic range of temperature. Initial brain perfusion was set at 0.019333 s^{-1}. Left: Comparison of extent of cooling of a 1-mm radius tumor from nearest probe surface in the x- (black) vs. z-axis (gray) of a coronal plane. Middle: Comparison of varying tumor (1.5-mm radius) perfusion relative to brain perfusion (0.73x, black to 3.96x, grey). Right: Varying heat energy withdrawal on cooling a 1.5-mm radius tumor. **(d)** Thermoelectric cooling device consisting of a lower Interface for tissue interface and an upper, removable Cooler for air-based heat exchange. **(e)** Exploded 3D render of thermoelectric device. Cooler consists of a fan, heatsink with cover, Peltier plate, and a base with a copper plate for thermal contact to Peltier and Interface (with thermal paste), and steel shims for thermistor contact. Interface consists of copper plate for thermal contact to Cooler, gold cooling probe as tissue interface, and thermistor with wires around insulated brass screws. Cooler is attached to the Interface by screws. **(f)** *In vivo* temperature measurement from the thermistor of the Interface, 1 mm from the probe. Here, both rats possessed a device, but only one was switched on (blue). **(g)** Representative MRI images of tumor growth on Day 0 (just prior to switching device on) and Day 14. Red bar images are with device off, blue bar images are device on. **(h)** Tumor volume measured from MRI and normalized to Day 0 volume. Mixed-effects analysis was conducted to compare the groups.

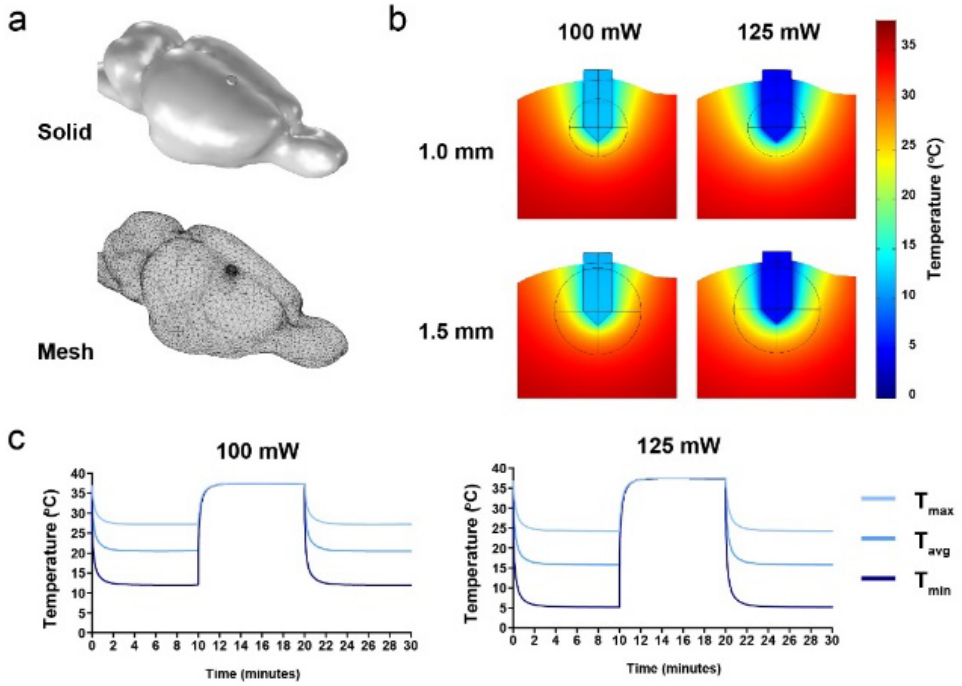

Supplementary Figure 4: Finite-element analysis of local intratumoral hypothermia. (a) Above: Smoothened rat brain model obtained from the literature. Below: fine mesh added to the model for finite-element analysis. **(b)** Coronal slices depicting degree and extent of hypothermia depending on tumor size (1 mm and 1.5 mm radius) and heat energy pulled (100 and 125 mW). **(c)** Time-dependent study modeling maximum, average, and minimum tumor temperatures over time. Cooling was begun at t = 0, stopped at t = 10, and restarted at t = 20 minutes.

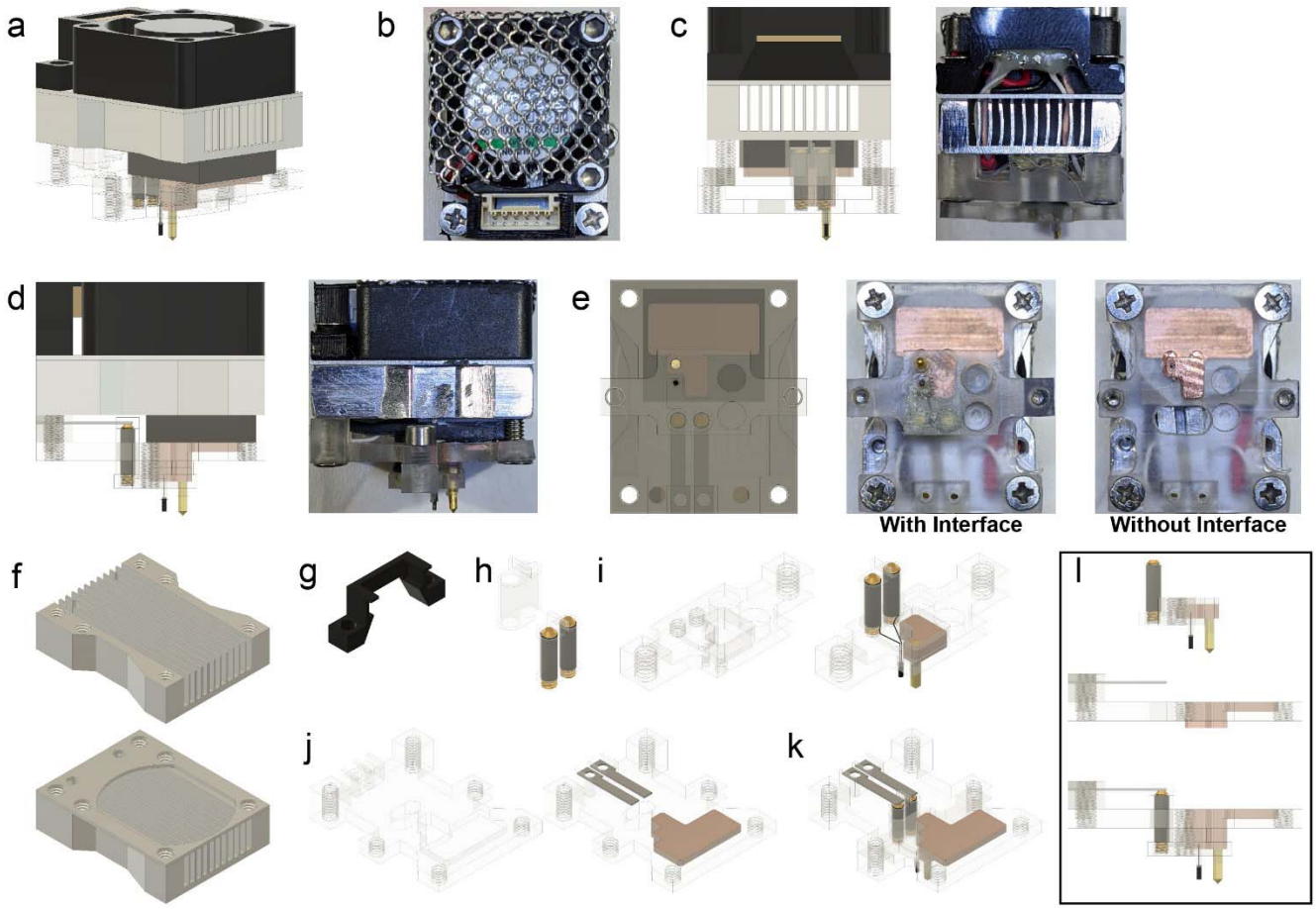

Supplementary Figure 5: Local hypothermia device. (a) Rendered front angle view of device. **(b)** Top view of device. Aluminum mesh is visible above a fan. Beige connector is visible surrounded by a 3D printed cover. **(c)** Rear view of device. Left: render. Right: picture shows wires terminating at connector where they were soldered and protected with epoxy. **(d)** Side view of device. All components are visible with this perspective. **(e)** Bottom view of device. Left: render. Middle: Picture including the presence of Interface. Right: Picture without the Interface. Steel shims, Peltier wires, and copper part are visible through the polycarbonate base. **(f)** Render of heat sink without cover (above) and with cover (below). Holes were drilled to enable passage of wires and fastening of screws. **(g)** Render of 3D-printed component to secure the beige connector. **(h)** Render of polycarbonate part to protect the heat-shrink covered brass screws. **(i)** Render of polycarbonate Interface base alone (left) and with all parts (right). Thermistor wires are wrapped around the brass screws under the heat shrink. Copper part with gold needle is pressed into the polycarbonate base. **(j)** Render of polycarbonate plate of Cooler alone (left) and with all parts (right). Steel shims are components of the thermistor circuit. **(k) and (l)** Renders of Interface and polycarbonate plate of Cooler as they are contacted together to enable heat conduction and closing the thermistor circuit.

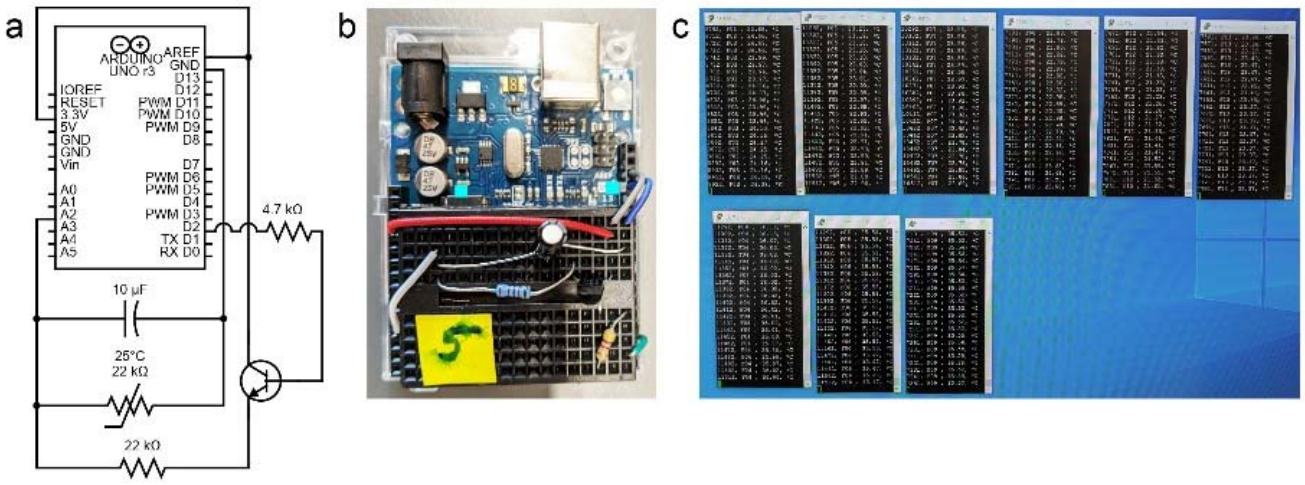

Supplementary Figure 6: Thermistor circuit for temperature monitoring. (a) Schematic demonstrating the voltage-divider circuit used to measure resistance across the thermistor. A digital pin from the Arduino was used to take intermittent and averaged recordings (every 10s). **(b)** Photo of voltage-divider circuit on a breadboard above the Arduino. One of these was used per rat for temperature monitoring. Arduino code converted the resistance across the thermistor to temperature using a manufacturer supplied beta-value. **(c)** Picture of computer screen depicting continuous temperature monitoring through PuTTY. The computer was also connected to the network to enable temperature monitoring outside the vivarium.

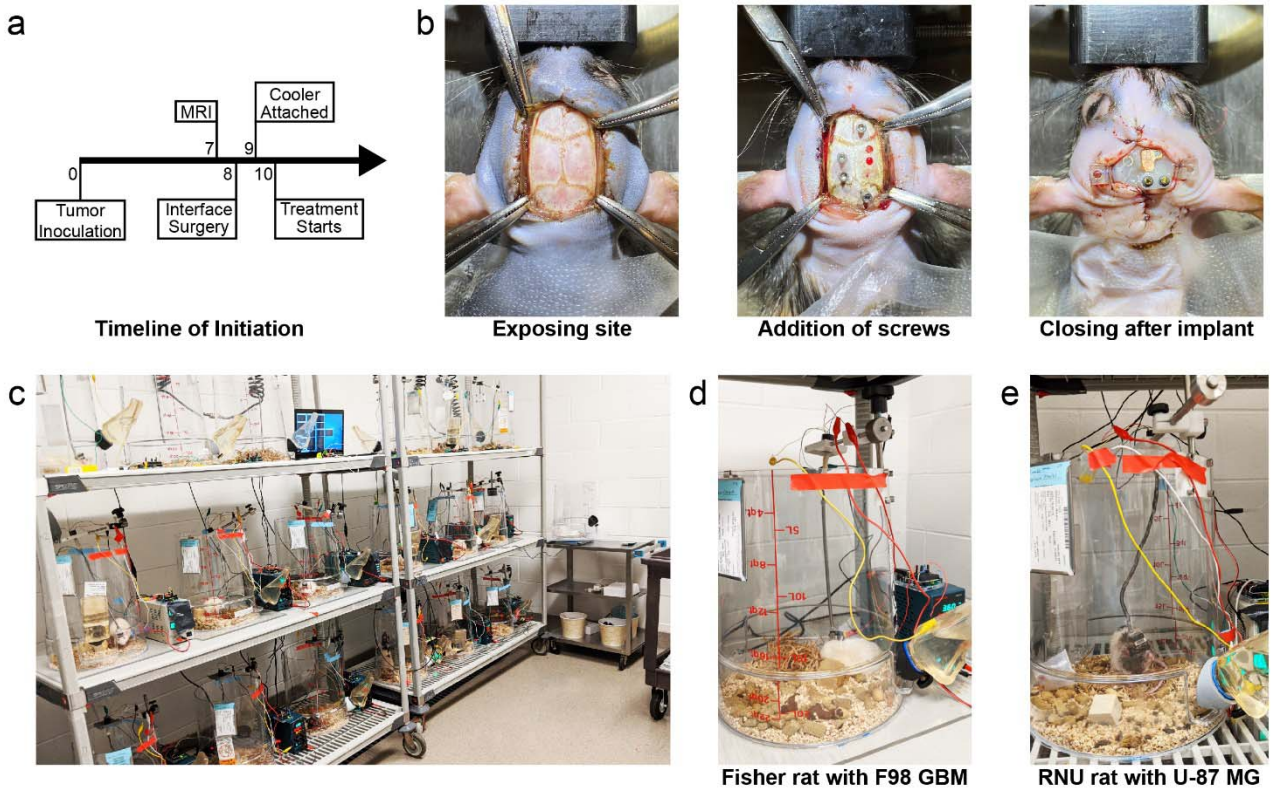

Supplementary Figure 7: *In vivo* Interface implantation and treatment application. (a) Timeline of tumor inoculation, MRI, Interface implant surgery, Cooler attachment, and treatment initiation. **(b)** Photos of implantation surgery in an RNU rat 8 days after tumor inoculation. Left: the surgical site is re-exposed and hemostasis established. Middle: burr holes were drilled for the intratumoral probe, thermistor, and four titanium screws. The titanium screws were tightened by hand. Right: suturing around the Interface which was attached to the skull using dental cement. The copper part for heat conduction and the brass screws are visible for contact with the Cooler. **(c)** Set up of multiple cages, power supplies, temperature monitoring, and a central computer in the vivarium. Rats were weighed in an empty cage

visible on the right. **(d)** Photo of a Fisher rat under treatment. Patch cable, slip ring, lever arm, power supply, and water bottle are visible. **(e)** Nude (RNU) rat under treatment.

d. Local cytostatic hypothermia extends survival of rodents with GBM in two models.

As local hypothermia reduced *in vivo* tumor growth rate in preliminary imaging studies, we investigated its effect on animal survival. In a model with the aggressive F98 line in Fischer rats, we investigated whether survival would increase despite being unable to reach cytostatic temperature for F98 (20°C). After confirmation of tumor-take with GFP^+ F98 cells (Supplementary Fig. 8a), Interface implantation (example in Supplementary Fig. 7b), and Cooler attachment, rats were randomly assigned to two groups. Half of the rats (n = 9) had their device switched on to deliver hypothermia while half (n = 9) remained off. Of the rats receiving hypothermia, only 2 reached near or below 20°C (Supplementary Fig. 8b), the cytostatic temperature observed for F98 cells. All rats not receiving hypothermia required euthanasia with a median time of 3.9 weeks (Fig. 4a). After a recovery phase, rats receiving hypothermia did not exhibit obvious signs of weakness or distress, maintained an appetite, and gained weight (Supplementary Movies 1 and 2, and Supplementary Fig. 8c). Rarely, a seizure was observed while switching on the device, which abated quickly on turning off and did not recur when gradually ramping up hypothermia over a few minutes. The implanted Interface of one rat broke off prematurely at week 7 leaving him without treatment for 1.5 days and the point was censored (Fig. 4a). The median survival for 6 treatment rats was 9.7 weeks (Fig. 4a) demonstrating a significant increase in survival ($p < 0.0001$). The remaining 2 rats that survived through the study period were the ones in which cytostatic hypothermia was achieved (Supplementary Fig. 8b). Histology demonstrated large tumors in normothermia rats (Fig. 4b), including one rat in which tumor was almost invisible on initial MRI (Supplementary Fig. 8a). Of the treated rats that eventually progressed to euthanasia, all had tumors growing away from the cooling probe (Fig. 4c). The two surviving rats did not show a mass (Fig. 4d) but a few GFP^+ cells were observed in histological sections (Supplementary Fig. 8d) which were not proliferative (Supplementary Fig. 8e).

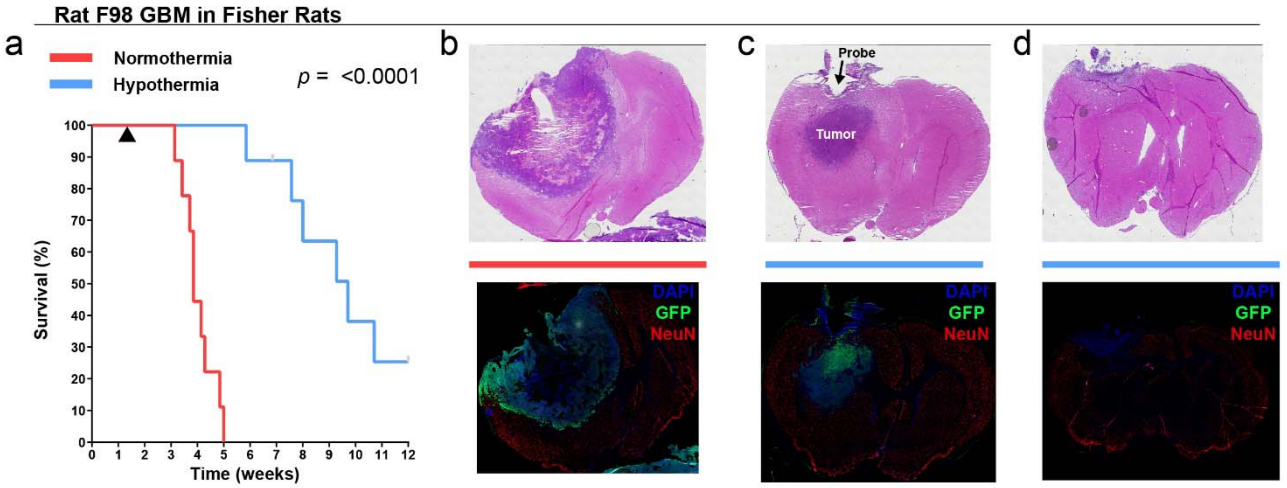

Figure 4: Delivery of local cytostatic hypothermia in Fisher rats with F98 GBM. (a) Kaplan-Meier survival plot of rats with the device switched off (red, n = 9) or switched on to deliver hypothermia (blue, n = 9). Gray bars indicate censored rats. Black triangle indicates the start of hypothermia treatment. Groups were compared with the log-rank Mantel-Cox test. **(b–d)** Coronal brain sections stained with H&E (top) and IHC (bottom) to show extent of tumor. **(b)** Representative from normothermia group. **(c)** Representative from hypothermia groups that reached euthanasia criteria. Tumor visible in the z-direction from probe **(d)** Representative section from hypothermia group that survived through study period.

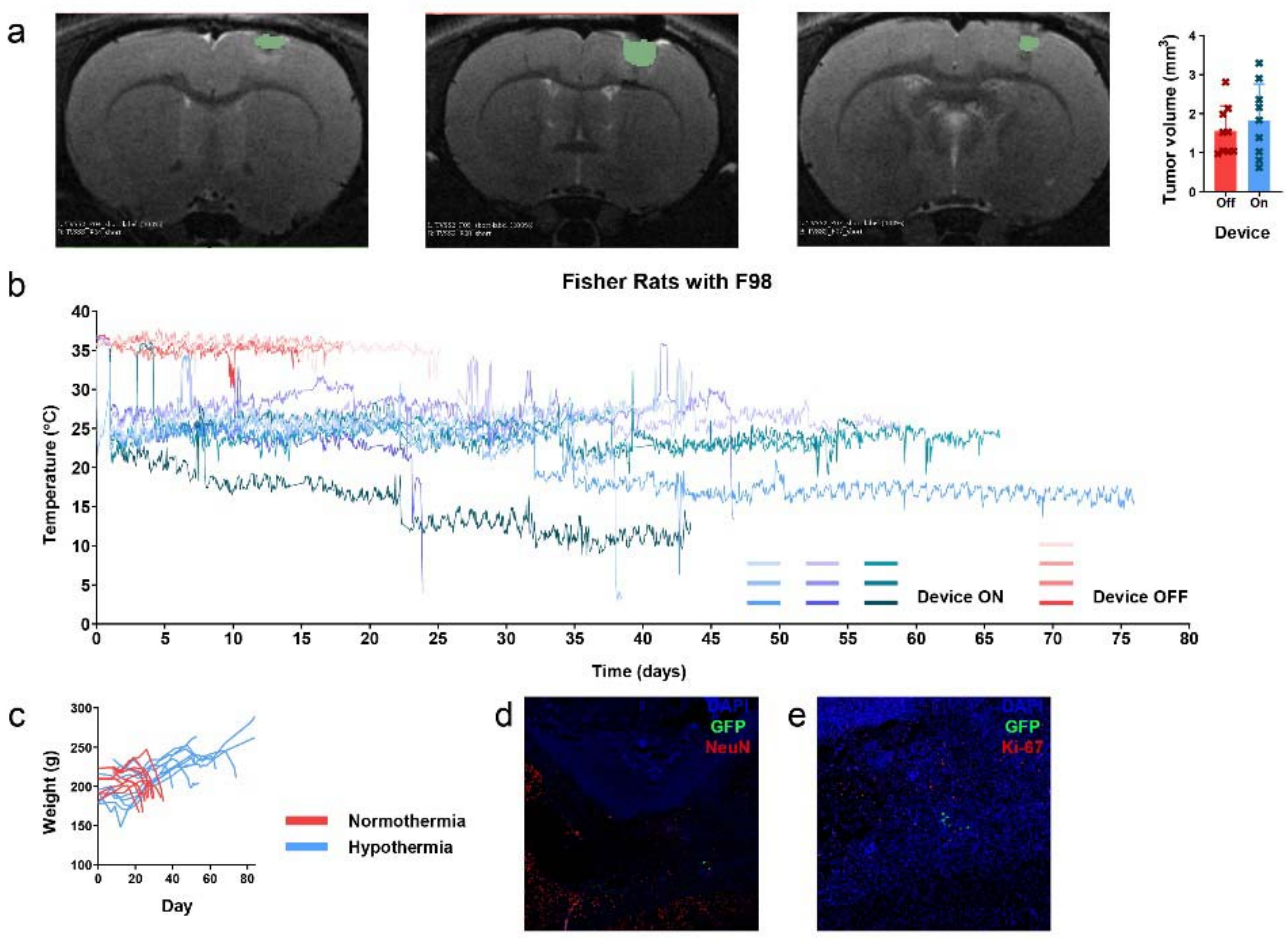

Supplementary Figure 8: Hypothermia treatment of Fisher rats with F98 GBM. (a) MR images 7 days after tumor inoculation confirming tumor development. Green mask represents tumor. Tumor volumes between the two treatment groups were not significantly prior to initiating treatment. **(b)** Continuous temperature monitoring of 9 rats with their device switched on and 4 rats with their device switched off. The remaining 5 normothermia rats did not have temperature monitoring. **(c)** Rat weights through the study period. **(d)** Histological section demonstrating the presence of some GFP^+ cells in one of the surviving rats. **(e)** Histological section demonstrating that GFP^+ cells in one of the surviving rats did not co-stain with Ki-67.

Next, we assessed cytostatic hypothermia on human U-87 MG grown in RNU rats. After confirmation of tumor-take (Supplementary Fig. 9a), Interface implantation (Supplementary Fig. 7b), and Cooler attachment, 6 rats had their device switched on and 5 were kept off (rats were randomly assigned to each group). The devices of 4 treatment rats reliably delivered 25°C hypothermia (Supplementary Fig. 9b), the cytostatic temperature observed for U-87 MG. The thermistors of two rats failed early and treatment of one may not have been reliably delivered ("N06"). All rats receiving normothermia required euthanasia with a median time of 3 weeks (Fig. 5a). As previously, the rats did not demonstrate signs of distress, had a strong appetite, and gained weight (Supplementary Movies 1 and 2, Supplementary Fig. 9c). However, these rats were highly active, and their devices and cables required frequent maintenance and replacement with intermittent failures. Because of this, Interface implants started to break off by the 7^{th} week, points were censored, and the study was terminated at 9 weeks (Fig. 5a). We attempted reimplantation in two rats (including "N06"), but this resulted in complications and days without treatment. None of the rats in the hypothermia arm died due to tumor growth within the study period (Fig. 5a) demonstrating a significant increase in survival (p = 0.0007). On histology, rats not receiving hypothermia had large tumors (Fig. 5b). In the rat that had an early thermistor failure ("N06") and the rat without treatment after re-implantation, a tumor mass was visible (Fig. 5c). The remaining hypothermia rats exhibited a

stable tumor burden without a separate mass (Fig. 5d). Together, these F98 and U-87 MG studies demonstrate that local delivery of cytostatic hypothermia can prolong survival.

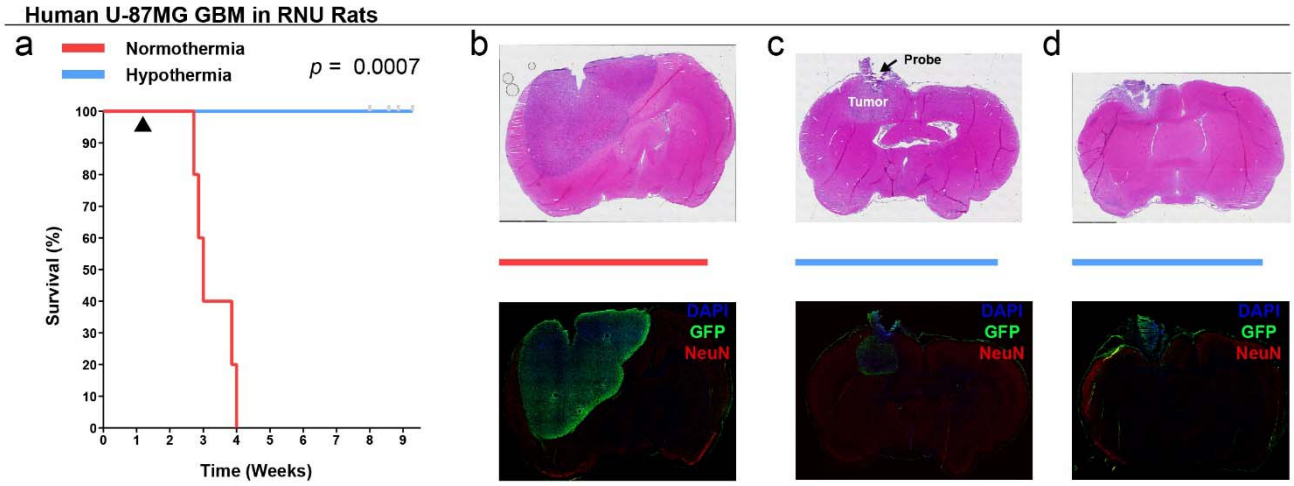

Figure 5: Delivery of local cytostatic hypothermia in RNU rats with human U-87 MG GBM. (a) Kaplan-Meier survival plot of rats with the device switched off (red, n = 5) or switched on to deliver hypothermia (blue, n = 6). Gray bars indicate censored rats. Black triangle indicates start of hypothermia. Groups were compared with the log-rank Mantel-Cox test. **(b–d)** Coronal brain sections stained with H&E (top) and IHC (bottom) to show extent of tumor. **(b)** Representative from normothermia group. **(c)** Representative from hypothermia groups that had poor treatment management or multiple device failures and grew a tumor in the z-axis (n=2). **(d)** Representative section from hypothermia group that did not grow a separate tumor mass (n=4).

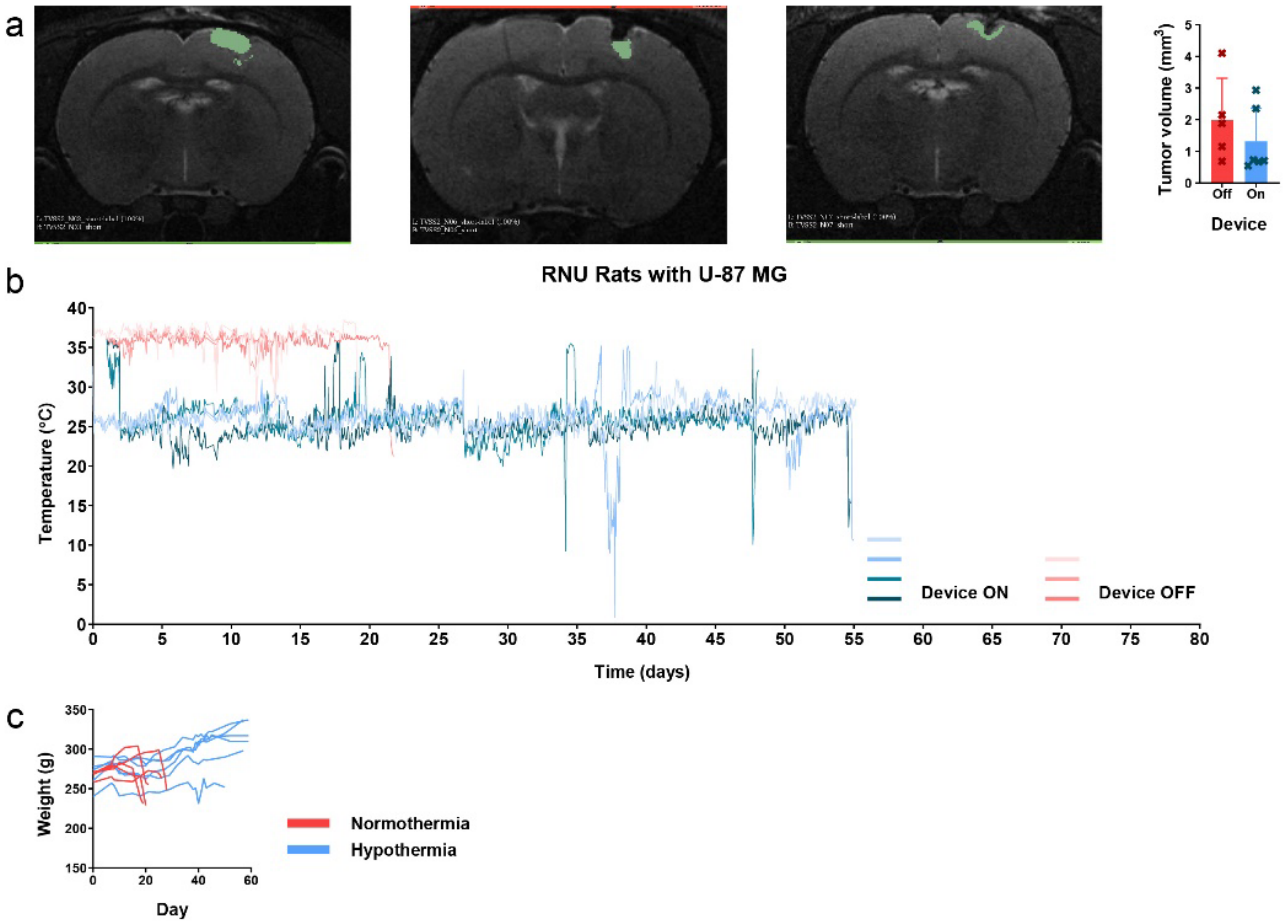

Supplementary Figure 9: Hypothermia treatment of Nude (RNU) rats with U-87 MG. (a) MR images 7 days after tumor inoculation confirming tumor development. Green mask represents tumor. Tumor volumes between the two treatment groups were not significantly prior to initiating treatment. **(b)** Continuous temperature monitoring of 4 rats with their device switched on and 3 rats with their device switched off. The remaining 2 treatment rats had premature failure of their thermistors with erratic readings and are thus not displayed. The remaining 2 normothermia rats did not have temperature monitoring. **(c)** Rat weights through the study period.

e. Cytostatic hypothermia can be effective with chemotherapy or CAR T immunotherapy *in vitro*.

We next assessed the effect of concomitant cytostatic hypothermia with temozolomide (TMZ) chemotherapy or CAR T immunotherapy *in vitro*. Human GBM lines received two TMZ doses at 37°C or 25°C followed by media replacement and incubation at 37°C. All three lines had reduced well coverage after 1000uM of TMZ compared to no TMZ (DMSO only) under 25°C (Supplementary Fig. 10a). Additionally, both TMZ and hypothermia halted cells in the G2-phase of the cell cycle (Supplementary Fig. 10b). U-87 MG growth was significantly reduced by combined TMZ and hypothermia pretreatment compared to TMZ alone (at 37°C) (Fig. 6a). Growth of T98G, a TMZ-resistant line, was significantly reduced by hypothermia alone and unaffected by 500 and 1000 µM of TMZ alone (at 37°C) (Fig. 6b). However, the combination of 500 or 1000 µM TMZ with 25°C hypothermia had significantly delayed growth by day 12. Similarly, LN-229 growth was significantly reduced by both TMZ and hypothermia individually, and the combination resulted in an enhanced effect (Fig. 6c).

We next investigated whether CAR T induced cytotoxicity (of EGFRvIII$^+$ CT2A GBM) was possible despite hypothermia reducing cellular functions. Expression of the chimeric antigen receptor on T cells enabled killing of GFP$^+$EGFRvIII$^+$ CT2A cells and not GFP$^+$EGFRvIII$^-$cells at 37°C (Supplementary Fig. 10c). In the absence of CAR T cells, CT2A cell growth was inhibited by both 24 and 20 h/d of 25°C hypothermia (Fig. 6d).

With the addition of 10,000 CAR T cells (5:1 ratio of T cell:tumor), tumor was eradicated within 24 hours at 37°C (Fig. 6e). Under 25°C hypothermia, 10,000 CAR T cells significantly reduced the tumor cell count to 25% of the original count within 24 hours and to <10% by 96 hours. Reducing the hypothermia dosage to 20 h/d further reduced the remaining tumor percentage (Fig. 6e). Reduced IFNγ was detected in the media when immune mediated killing took place under hypothermia (Fig. 6f). Adding a second dose of CAR T cells after 24 hours brought the remaining tumor to <5% of the original seeding (Fig. 6g). Pretreating CT2A cells with 25°C hypothermia for 4–7 days reduced their subsequent growth rate at 37°C (Fig. 6h, left). However, this reduced their susceptibility to CAR T cells at 37°C (Fig. 6h, middle) and 25°C (Fig. 6h, right).

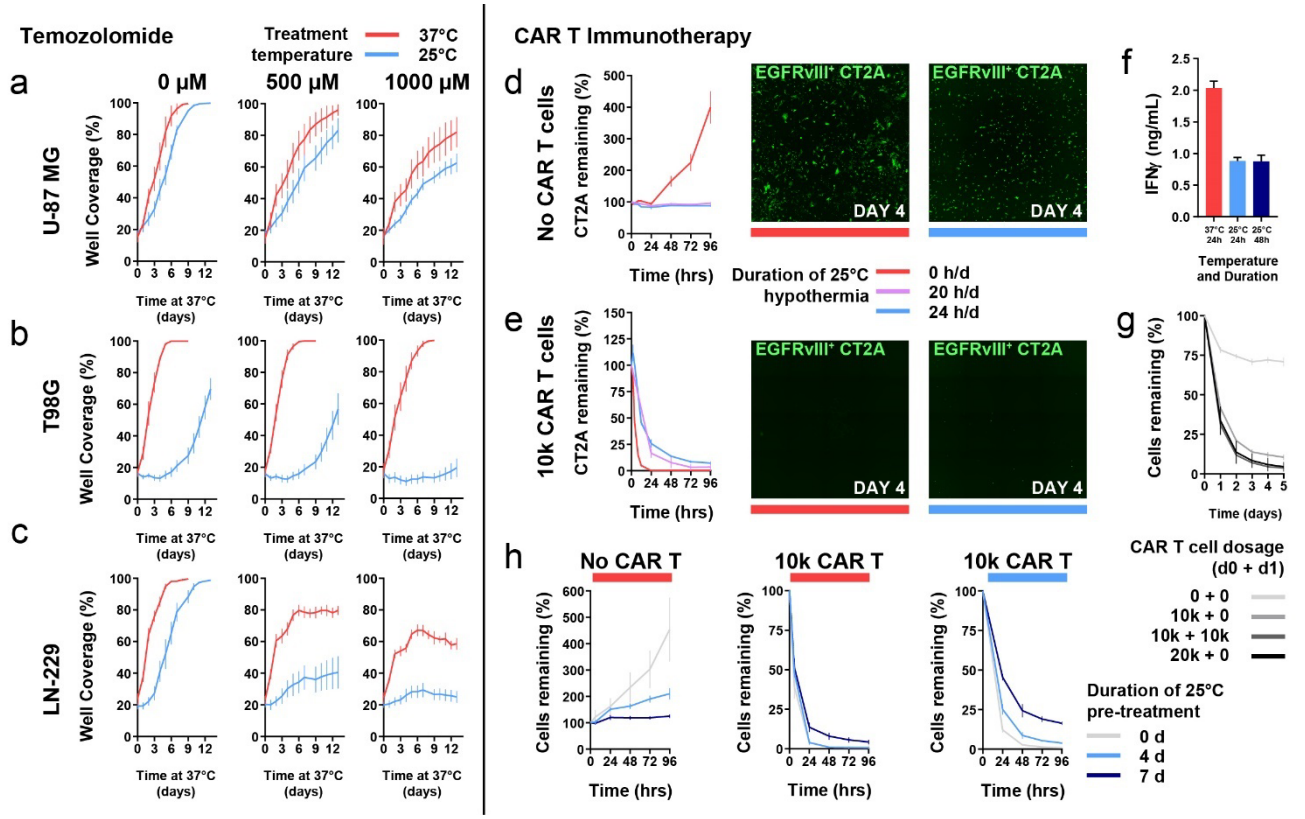

Figure 6: Use of cytostatic hypothermia with chemotherapy and CAR T immunotherapy. (a–c) Growth curves of U-87 MG, T98G, and LN-229 with concomitant TMZ chemotherapy (DMSO only or 500 and 1000 µM TMZ) and hypothermia. Red line represents pre-treatment with TMZ at 37°C while blue line represents pre-treatment with TMZ at 25°C. Plotted lines show growth curves after the final wash of media to remove TMZ, both at 37°C. Two-way ANOVA with Sidak's post-hoc test demonstrated significant differences between the 37°C and 25°C groups on day 13 in **(a)** U-87 MG at 500 µM ($p < 0.05$) and 1000 µM ($p < 0.05$), **(b)** T98G at 500 µM ($p < 0.0001$), and 1000 µM ($p < 0.0001$), and **(c)** LN-229 at 500 µM (($p < 0.0001$), and 1000 µM (($p < 0.0001$). **(d–e)** GFP$^+$ EGFRvIII$^+$ CT2A tumor cells remaining after treatment without **(d)** and with 10,000 CAR T cells **(e)** under normothermia, or continuous or intermittent hypothermia (20 h/d). Representative images of remaining tumor cells at day 4 after beginning treatment. **(f)** IFNγ quantification from media with EGFRvIII$^+$ CT2A cells and CAR T cells. One-way ANOVA with Dunnett's post-hoc test demonstrated a significant difference ($p < 0.0001$) between the 37°C and each of the 25°C groups. **(g)** Remaining CT2A cells with higher or multiple CAR T cell dosage over 2 days. **(h)** Remaining CT2A cells after pretreatment with 25°C hypothermia for 0, 4, or 7 days, followed by addition of 0 or 10,000 CAR T cells, and plate moved to either 37°C (left and middle) or 25°C (right).

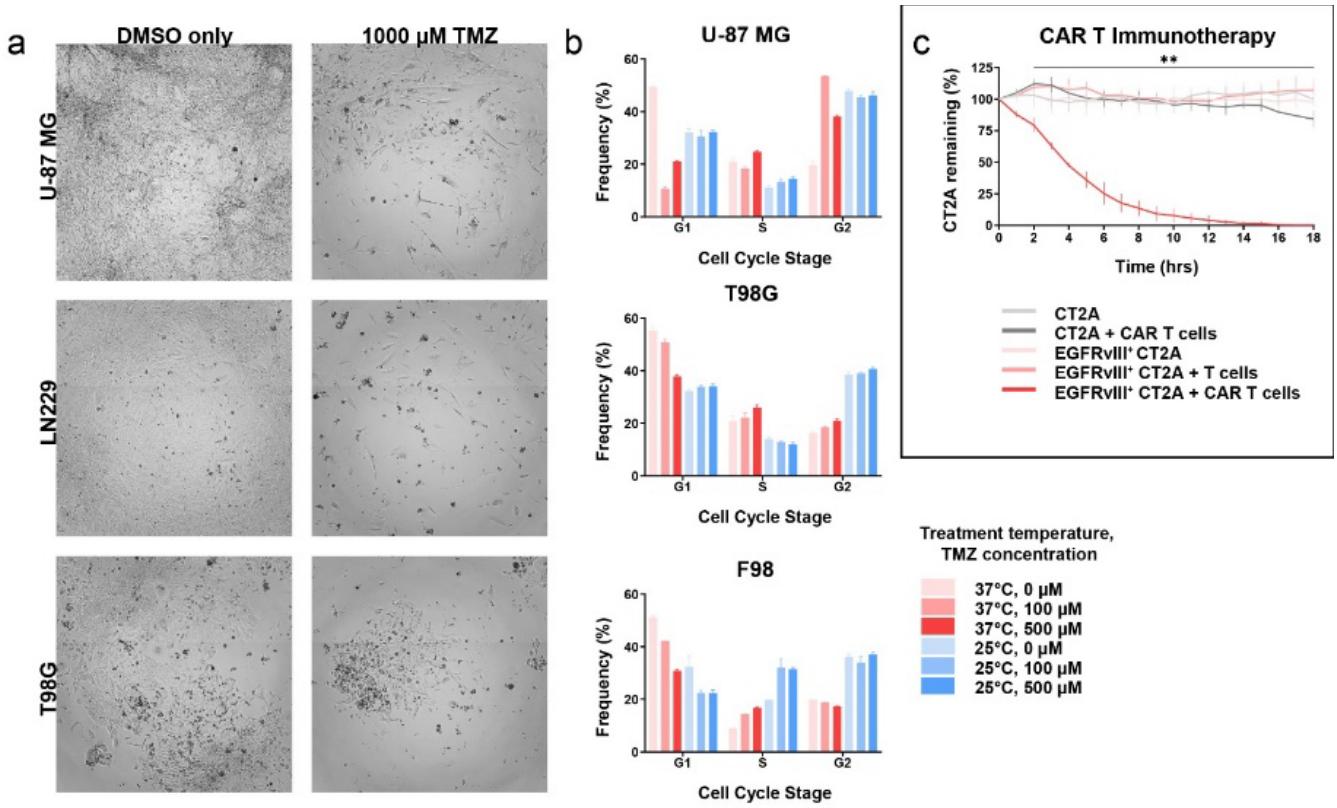

Supplementary Figure 10: Effect of cytostatic hypothermia on TMZ and validation of CAR T cells. (a) Brightfield images representing U-87 MG, LN-229, and T98G treated with DMSO only or 1000 μM TMZ in DMSO. These images were taken 12 days after TMZ was removed. **(b)** Effect of TMZ and hypothermia on cell cycle progression. U-87 MG (above), T98G (middle), or F98 (bottom) were assayed immediately after TMZ treatment under 37°C or 25°C. **(c)** Graph demonstrating the specific killing of EGFRvIII$^+$ CT2A cells by CAR T cells only. Repeated measures ANOVA was conducted with Dunnett's multiple comparisons test comparing the group of EGFRvIII$^+$ CT2A cells with CAR T cells to EGFRvIII$^-$ CT2A only (**p<0.01 at least in all comparisons).

3. DISCUSSION

These studies demonstrate the potential of local hypothermia for managing glioblastoma. Through regimented *in vitro* studies, we defined a window of growth-halting temperatures, assessed their effects on cells, and explored strategic intermittent timelines to improve the logistics of implementation. We modeled and successfully fabricated device prototypes to administer and monitor local hypothermia, including one which was MR imaging compatible. In two rodent models of GBM, local hypothermia extended survival while permitting the animals to behave normally and eat and move freely (Fig. 4 and Supplementary Movies 1 and 2). This work also suggests that in patients, local hypothermia could work with adjuvants and may provide opportunities to assess novel therapies. We suggest that the window of safe but growth-halting temperatures we term 'cytostatic hypothermia' will be a critical addition to the clinical options available to patients with GBM.

We established cytostatic temperatures ranging from 20–25°C (Fig. 1b and Fig. 6d) for 5 cell lines. This corroborates previous findings describing reduced cell division at hypothermic temperatures[14,23–27]. Intriguingly, unlike most lines we tested, F98 cells required 20°C hypothermia to halt division (Fig. 1b). In fact, F98 cell morphology also significantly differed between 25°C and its cytostatic temperature of 20°C (Supplementary Fig. 2d and e). All cell lines, including F98 above its cytostatic temperature, demonstrated that cells accumulate in the G2-phase (Fig. 2a), corroborating prior studies[24,25]. A decrease in viability was also apparent in our Live:Dead and growth assays across the human GBM lines (Fig. 1d and e). In the context of cytostatic hypothermia, cell death is not the goal as healthy cells, although more resilient to hypothermia[24], may die too. Mechanisms of death could include an accumulation of Na^+ or Ca^{2+} or increased aquaporin-4 expression[29–31] and subsequent swelling. To circumvent this, intermittent hypothermia may be equally cytostatic (Fig. 1c) but less cytotoxic.

Next, we performed a preliminary investigation of cellular metabolism and aimed to assess whether F98 has pathways that are more resilient to 25°C hypothermia. Accumulating ATP in most lines (Fig. 2b) suggested that ATP consumption diminished more than production. This corroborates findings in hepatocytes that elucidated differences in specific metabolite production vs. consumption sensitivity to hypothermia[32]. In our metabolite survey, we observed that production and consumption of 4 metabolites decreased regardless of the degree of hypothermia (Fig. 2c and Supplementary Fig. 3). This is of particular interest when considering dietary and pharmaceutical efforts to reduce glucose consumption and lactate production to starve a tumor of resources[33–35]. Cytostatic hypothermia provides a means to reduce both metabolites, but instead by decreasing the tumor's appetite for nutrients. However, deeper studies of the metabolic profile under cytostatic hypothermia are needed to understand whether they can explain why F98 has a colder cytostatic temperature. Additionally, the transcriptome is affected by hypothermia as well—cardiomyocytes cultured at 28°C showed 2413 differentially expressed genes[36]—and further study is warranted.

The reduction in inflammatory cytokines, IL-6 and IL-8, under hypothermia (Fig. 2c) is of interest as these cytokines are strongly associated with glioblastoma invasiveness[37]. Similarly, the absence of anti-inflammatory cytokine secretion is reassuring. However, reduced cytokine production also affected CAR T cells wherein reduced IFNγ production (Fig. 6f) was correlated with reduced cytotoxicity (Fig. 6e). Hypothermia pre-treatment of tumor also affected CAR T efficacy (Fig. 6h), warranting an investigation of tumor surface marker changes. Nevertheless, despite this reduction, CAR T cells significantly reduced the tumor cell count over 4 days under persistent cytostatic hypothermia (Fig. 6e). Intermittent hypothermia improved the efficacy. These results suggest a paradigm of CAR T treatment under normothermia, with local cytostatic hypothermia in between doses to prevent tumor progression. Thus, the data demonstrate that immune cells may still be cytotoxic in early phases of hypothermia, and efficacy can be enhanced by intermittent warming.

Cytostatic hypothermia was also synergistic with standard-of-care TMZ chemotherapy *in vitro* (Fig. 6 a–c), and may facilitate radiotherapy as well[38]. T98G cells are resistant to TMZ due to the enzyme MGMT[39]. Interestingly, we observed that TMZ and cytostatic hypothermia together reduced growth of all three cell lines tested. The mechanisms behind this combined effect remain to be elucidated but may include increased hydrolysis of TMZ to its active ion, reduced MGMT expression, or other compromising effects of hypothermia. These results provide early rationale for combination strategies with current standards-of-care, particularly in the case of TMZ-resistant tumors.

Importantly, to the best of our knowledge, this report is the first attempt at *in vivo* delivery of cytostatic hypothermia to retard tumor growth and prolong survival. Despite multiple technical challenges, statistically

significant prolonged survival was observed in two rat GBM models (Fig. 4a and Fig. 5a). Promisingly, the two F98-inoculated Fisher rats that successfully received cytostatic hypothermia fully survived the study period. Although a few F98 cells were discovered upon histology (Supplementary Fig. 8d), they lacked Ki-67 and thus were not proliferating (Supplementary Fig. 8e). Furthermore, no RNU rats with human U-87 MG receiving cytostatic hypothermia required euthanasia due to tumor growth under treatment.

The therapeutic effects observed were likely possible due to the brain's resilience to hypothermia. Intracranial cryoprobes in patients and primates have been safe[14,16,19,21,22]. Additionally, cooling feline cortex down to 3°C, 2 h/d for 10 months showed neuronal preservation and minimal histological changes[18]. Interestingly, cooling the feline visual cortex intermittently for >3 years also demonstrated no histological changes, and visual evoked potentials were fully intact above 24°C and absent only below 20°C[19]. Coincidentally, our data demonstrated all GBM lines halted between 20–25°C. Our studies are likely the first to demonstrate the effects of *persistent* hypothermia. We observed that rats generally behaved 'normally': they responded to stimuli, ate food, gained weight, and moved freely (Supplementary Movies 1 and 2). In all our studies combined, seizures were observed a few times but were easy to abate. Other adverse effects of hypothermia are possible via transiently reduced neural activity and cellular swelling. However, these may be solved by gradually changing temperature, intermittent hypothermia, administering molecular inhibitors[29–31], and the use of adjuvants to reduce the total length of therapy. More precise long-term effects of continuous cytostatic hypothermia remain to be studied. This should include investigating subtle functional abnormalities, as well as an assessment of plasticity-induced compensation over time.

Given our findings, we suggest that local cytostatic hypothermia comes with translational advantages. Unlike targeted therapeutics, cytostatic hypothermia affects multiple cellular pathways simultaneously (Fig. 2). Additionally, the reduced rate of cell divisions likely reduces the occurrence of new mutations. Hence, the development of resistance and progression becomes more unlikely. In fact, cytostatic hypothermia could also be delivered using a paradigm of 'Adaptive Therapy', further reducing the chance of resistance. In such paradigms, treatment dosage is adjusted to maintain a burden of chemosensitive cells[40] to limit growth of more aggressive chemoresistant cells. These strategies have improved survival in animal models and patients[41]. Nevertheless, by leveraging physics, the mechanisms behind the therapeutic response of cytostatic hypothermia are unlikely to differ dramatically between species (e.g., rats and humans). Thus, its biological and therapeutic effects are likely to translate to patients.

The one significant translational challenge that remains is designing a patient-centric local cytostatic hypothermia device. To induce hypothermia, heat energy must be transported out of the tissue. In the middle 20th century, this was attempted through a cryoprobe tethered to an external refrigerator[14]. Today, variations of this approach exist, some of which use Peltier plates[19,21,42–45]. However, all require heat removal via percutaneous device components that would be susceptible to infection (in patients that may already be immunocompromised). In our rodent studies, our device design had an external heat sink and fan. This air-based convection was inefficient and reliable cooling was limited to ~25°C (Fig. 3f). Future designs may use fluid-based heat transfer to improve efficiency, be MRI-compatible for regular tumor progression monitoring, and be fully implantable. Our computational studies demonstrated that cooling was less effective in the z-axis (Fig. 3c). Corroborating this, rats that grew a tumor mass under treatment, grew it below the probe (Fig. 4c and Fig. 5c). Additionally, the model demonstrated perfusion of the brain kept cooling relatively local, corroborating the literature[42]. This makes cooling a large region of tissue difficult, but also protects distant parts of the brain. However, we used a single probe in our model and device Interface. While effective at this scale, additional probes could enable homogenous cytostatic hypothermia in a larger volume of tissue with minimal tissue displacement. Promisingly, cell lines did not require 24 h/d cooling to slow growth, with two lines (LN-229 and T98G) not showing any growth even under 18 h/d (Fig. 1c and Supplementary Fig. 2b). Given that tumors grow more slowly *in vivo*[46], a therapeutic device may not need to be powered 24 h/d to maintain cytostasis. Based on these findings, we conclude that our data motivate the design of a fully implantable local cytostatic hypothermia system for the treatment of GBM.

Overall, we have provided evidence of the utility of local cytostatic hypothermia for slowing the growth of GBM. We demonstrated that cytostatic temperatures curb growth of GBM *in vitro*, and these results were corroborated *in vivo*. Mechanisms that remain to be investigated include those governing differential cell sensitivity to hypothermia and synergism with concomitant therapies. These could include transcriptomic and

metabolomic analyses across grades of hypothermia and patient-derived tumors from the brain and other organs. Our fabricated device could be used with novel temperature-sensitive polymers for tumoral drug delivery[47] or for CAR T homing[48]. However, advancing the technology to be fully implanted could enable treating intracranial tumors in patients, and tested against other tumors of other organs that are susceptible to hypothermia[23–27]. Ultimately, this therapeutic domain could indefinitely prolong survival (by maintaining a tumor burden, like via Adaptive Therapy), or used intermittently with current and novel cytotoxic strategies to eliminate GBM. Regardless, local cytostatic hypothermia could serve as a critical addition to the few options patients with GBM have.

4. MATERIALS & METHODS

a. Cell Culture

All cell lines were purchased from either ATCC or the Cell Culture Facility at Duke. To simplify culturing and passaging, all cells were progressively adapted to a unified medium: Dulbecco's MEM (Corning 10-013-CV) + NEAA (Gibco) + 10% FBS (Gemini Bio). For metabolite assays, DMEM (Corning 17-207-CV) was supplemented with 5mM Glucose (Gibco), 2 mM Glutamine (Gibco), 1 mM Na^+ Pyruvate (Gibco), and 10% dialyzed FBS (Gemini Bio 100-108). These media might affect growth rates for individual lines and thus future studies may scrutinize growth under different media formulations under cytostatic hypothermia. Cell lines were passaged twice after thawing for recovery and then used within 5 passages for all experiments. To dislodge cells, 0.05% trypsin (Corning 25-052) was used for U-87 MG and F98, while 0.25% trypsin (Corning 25-053) was used for LN-229 and T98G. Cells were counted using an automated cell counter (Countess II, Invitrogen) calibrated to manual cell counts for each cell line. Cells were plated at a density ranging from 1,000–20,000 cells/well in clear-bottom 96-well plates (Falcon 353219) depending on the desired confluence at the start of the assay. Plated cells were always incubated overnight at 37°C to ensure adherence prior to any experiment. A HeraCell CO2 incubator was used for all experiments at 5% CO2 and set at either 37, 30, 25, or 20°C. Media was carefully replaced every 2–4 days. To prevent losing cells from plates, multi-channel pipettes were used to suction media instead of a vacuum.

b. Imaging and analysis

Imaging was performed on a live-cell microscope (DMi8, Leica Microsystems) with a built-in incubator and CO2 regulator. Well plate dimensions were added to the microscope software (LASX) to enable tile scanning. Images were taken at 5X with a 2X2 field with 25% overlap in 96-well plates. For lengthy imaging periods (>10 min/plate), the incubator and CO2 regulator were used. For analysis, images were merged without stitching as low cell counts prevented accurate automatic stitching. Images were then analyzed through a custom automated ImageJ script to quantify the area coverage of a well plate. To obtain cell morphology (circularity and average size), the script was modified to analyze single cells. For fluorescent live/dead cell detection, an EarlyTox Live/Dead Assay kit was used (Molecular Devices) and the microplate was imaged with a laser and GFP and TXR filters. For immunotherapy experiments, images were taken at 10X with a 4X4 field and a laser through a GFP filter. The ImageJ script was modified to count the number of GFP^+ cells. All analyzed images were then processed through custom Python scripts to organize the data for analysis.

c. Molecular assays

Cell cycle analyses were conducted with a Propidium Iodide Flow Cytometry kit (ab139418, Abcam). Samples were run on a flow cytometer (Novocyte 2060, ACEA Biosciences). Data was analyzed on FlowJo v10.7.

Intracellular ATP was detected from homogenized cells via a Luminescent ATP Detection Assay kit (ab113849, Abcam). Luminescence was detected in a microplate reader (SpectraMax i3x, Molecular Devices).

Metabolites were detected from media through luminescent based assays. Cells were grown in four plates with modified media at 37°C overnight and then media was replaced. All plates were then left for 3 days at 37°C after which media was collected and stored at -80°C from one plate and replaced in the others. Three plates were then moved to either 30, 25, or 20°C. Media was collected, stored at -80°C, and replaced every 3 days. Images were taken in a live-cell microscope prior to collecting media. Glucose consumption (Glucose-Glo, J6021, Promega), Lactate production (Lactate-Glo, J5021, Promega), Glutamine consumption (Glutamine/Glutamate-Glo, J8021, Promega), and Glutamate production (Glutamate-Glo, J7021, Promega) were assayed from diluted samples. Luminescence was detected in the microplate reader and calibrated to a standard curve of each metabolite. Data was normalized to well coverage area quantified from images and a custom ImageJ macro.

For cytokine analysis, cells seeded in 24-well plates at different densities for the 37°C and 25°C plates to reach similar confluence at the time of the assay. All plates were incubated overnight at 37°C and then incubated for 3 days at their respective temperature. Media was then collected and stored at -80°C from one plate. The media in the remaining plates were replaced and the plates were moved to 25°C. Media was then collected, stored,

and replaced every 3–4 days. Cytokines were detected from media samples with a custom multi-plex ELISA kit (LEGENDplex, BioLegend) and our flow cytometer (Novocyte 2060).

d. Adjuvant studies

Chemotherapy: Temozolomide (Sigma Aldrich) was dissolved in DMSO at 20 mg/mL and stored at -20°C in aliquots. Aliquots were used within 2 months. For these assays, cell lines were grown in the microplate overnight. Then a 37°C plate received TMZ treatment for 3 days (or DMSO only at the concentration used in the 1000 µM TMZ group). A second microplate was moved to 25°C TMZ was added after 2 days for 3 days. After TMZ treatment, the media was completely replaced, and the plates were moved back to 37°C with daily imaging in a live-cell microscope.

Immunotherapy: Briefly, using a previously described protocol[49], CAR T cells were generated by harvesting splenocytes from mice, and transducing them with a retrovirus that induces CAR T expression specifically targeting EGFRvIII on CT2A tumor cells. CAR T cells were stored in liquid nitrogen 4 days post-transduction. All experiments used CAR T cells 5–7 days post-transduction. For immune killing assays, 2000 $EGFRvIII^+$ GFP^+ CT2A cells were grown per well overnight in modified DMEM media as described previously. In pre-treatment studies, these plates were incubated for 4 or 7 days at 25°C. For experiments, different dosages of CAR T cells were added the following day with phenol red-free RPMI media and microplates were incubated at either 37 or 25°C. Microplates were imaged at regular intervals as described previously. The number of GFP^+ cells was quantified through an ImageJ macro.

e. Device fabrication

Device design and manufacturing was done in collaboration with the Pratt Bio-Medical Machine Shop at Duke University. Designs were developed on MasterCam and Fusion360 (Supplementary Fig. 5). Most materials and parts were obtained through McMaster, or vendors such as Digi-Key, Newark Element, Mouser, or Amazon.

Metal and polycarbonate parts: MasterCam designs were programmed into tool paths for a three axis CNC milling machine. Raw polycarbonate (McMaster), copper (145 copper, McMaster), and aluminum (McMaster) were used to fabricate various parts including the Interface, copper contacts, and the heat sink and its cover (Supplementary Fig. 5f). The tools used were .125", .0625" and 1 mm high speed steel end mills and high-speed steel drills.

Interface: This consisted of a polycarbonate base, a gold needle threaded through a copper part, and a thermistor with its ends wrapped around protected brass screws (Supplementary Fig. 5h and i). The gold needle was fashioned from 24k 1-mm diameter gold wire (Hauser & Miller) with one end sharpened to a 45° angle by hand with a fine jewelers file in a small lathe using a 1-mm 5C collet. The gold was inserted through a hole in the adjoining copper part, ensuring the proper length for tumor penetration (3 mm from bottom surface of polycarbonate base). The gold was carefully soldered to the copper with minimal 40/60 standard solder into the top side. Care was taken to prevent (and remove) any excess solder wicking past the gold to ensure proper seating into the base recess. Remaining gold and solder on top were filed flush to the copper.

Next, two brass screws were inserted into the polycarbonate base and fixed with epoxy (Henkel Loctite, Ellsworth Adhesives). Then, under a dissection microscope, thermistors (Amphenol Advanced Sensors) that were either MRI-compatible (A96N4-GC11KA143L/37C) or MRI-incompatible (AB6N2-GC14KA143E/37C), were measured, cut, and stripped with a blade. The thermistors were threaded through a hole in the polycarbonate base on one end, and the wires were wrapped around the brass screws. Heat shrink was added around the wired screws, and then protected with a polycarbonate part and secured with additional epoxy. Prior to implantation, these were sterilized under UV light for 30 minutes and left in 70% ethanol overnight.

Cooler: The Cooler (Supplementary Fig. 5a–e) consisted of a fan (MF20080V1-1000U-A99, Sunon), the fabricated heat sink with cover, a female connector (SM06B-GHS-TB, JST Sales America) protected by a 3D printed component (Supplementary Fig. 5g), a potted Peltier plate (TE-65-0.6-1.2, TeTech), and a fabricated polycarbonate plate with a copper part and steel shims (Supplementary Fig. 5j). The Peltier plate had thermal paste (Kryonaut, Thermal Grizzly) applied on both surfaces. An aluminum grill (9305T92, McMaster) was added above the fan to protect it from bedding. The Cooler was held together with screws.

Wiring: 26G wire was wrapped around screws that fastened the shims to the polycarbonate plate. These wires, along with the Peltier plate wires were passed through holes in the aluminum heatsink. The wires, including from the fan, were soldered to the female connector. The connector was protected with a 3D-printed part and then secured with epoxy and hot glue.

The device enabled the Cooler to be attached to the Interface such that the copper parts made contact to transfer heat, and the steel shims contacted the brass screws to complete the thermistor circuit (Supplementary Fig. 5k and l).

f. Caging and treatment set-up

To enable the free movement of awake rats under treatment, a custom caging and treatment setup was developed.

Cage and lever-arm: Rat housing was constructed by flipping 22qt plastic containers (Cambro) which were made hollow by sawing off the closed end. They were then sealed onto ¼"x15"x15" acrylic sheets (TAP Plastics) with cement for plastic (7515A11, McMaster). Parts were 3D printed to hold a water bottle and a lever arm. The two-axis lever arm consisted of 3D printed parts holding ¼" steel rods (McMaster) and a custom-made counterweight.

Electrical/treatment: Patch cables were made with male connectors (GHR-06V-S, JST Sales America) on either end of 12" jumper cables (AGHGH28K305, JST Sales America). These were protected by a spring (9665K84, McMaster) and the joints strengthened with epoxy and hot glue. A slipring (736, Adafruit Industries), to enable free rotation, had a female connector soldered and epoxied to an end hovering inside the cage. The patch cable connected the slipring to the Cooler.

Outside the cage, a variable voltage power supply (HM305, Hanmatek) was connected to the slipring with alligator clips. Each one powered the Peltier plate in one Cooler. USB 5V adapter towers (Amazon) were used to power the fans of multiple Coolers and connected with a USB jack on one end and alligator clips to the slipring on the other. Arduinos (Uno Rev 3, Arduino) connected to a laptop (through USB adapter towers) were connected to sliprings through a voltage-divider circuit on a breadboard and alligator clips. One Arduino was used per device for temperature monitoring.

g. Animals

All animal procedures were approved by the Duke IACUC. Fisher (CDF) and Nude (RNU) rats were purchased from Charles River at 7–9 weeks of age. All procedures began at 8–10 weeks of age.

Tumor inoculation: Tumor cells were grown *in vitro* for two passages, harvested the morning of the surgery, and kept on ice until injection. Animals were induced with 5% isoflurane anesthesia and maintained between 1–3% with visual monitoring of breathing. Buprenorphine-SR was administered subcutaneously at 1 mg/kg for pain control. Fur on the scalp was trimmed with an electric trimmer followed by removal with hair-removal cream. The head was then secured in a stereotaxic apparatus. Eye ointment was applied on the eyes. The scalp was sterilized with three alternating washes of 70% ethanol and chlorhexidine. Bupivicaine (0.25% w/v) was injected into the scalp. A central incision was made on the scalp and the skin retracted. A 0.6 mm conical burr was used to drill at -0.5 AP and + 3 ML to a depth of 0.8–0.9 mm. A Hamilton syringe with 26G needle loaded with at least 5 µL of either F98 cells (in Fisher rats) or U-87 MG cells (in RNU rats) was centered to the drill site. Prior to insertion, the tip was wiped of any hanging droplet. The needle was penetrated to a depth of 1.75 mm from the outer table of the skull and then retracted by 0.25 mm for a final location of 1.5 mm DV. Infusion was begun with a pump at 0.5 µL/min for 10 min. Upon 1 minute after completion, the syringe was slowly retracted, and the scalp sutured. The rat was then placed in the custom cage to begin accommodating. Supplemental nutritionally complete diet gel (76A, ClearH2O) was provided regularly.

Implantation: One week after inoculation, MR images were acquired was taken to confirm tumor-take. The subsequent day, the rats were prepared for implantation (Supplementary Fig. 7b). As previously, the rats were induced under anesthesia and buprenorphine-SR was administered subcutaneously at 1 mg/kg. The scalp was sterilized, bupivacaine (0.25% w/v) was administered, and the scalp was incised. This time, extra effort was put into retraction, scraping off the peritoneum, slightly separating the temporalis muscles, and ensuring hemostasis with etching gel (Henry Schein) and 0.4% hydrogen peroxide. Once the cranium was absent of blood and dry,

burr holes were made using conical drill bits (Roboz Surgical Instruments Co.) for the gold probe, thermistor, and titanium screws (0035962, Allied Titanium). This included one burr hole with a 0.8 mm tip for the thermistor, 1.5 mm caudal from the tumor inoculation. Following this, a 1.0 mm conical burr was used 6 mm laterally from the thermistor for titanium screw (TS) 1, 4 mm caudally from TS1 for TS2, 10 mm caudally from thermistor for TS3, and 6 mm rostrally from the tumor inoculation for TS4. The original tumor inoculation burr hole was expanded to 1.4 mm. Titanium screws (filed down to be 1-mm in length) were then twisted into their holes at a depth of 0.6 mm. Next, after cleaning the skull again, the sterile Interface was gently inserted and held down while UV-curable dental cement (Henry Schein) was added to the sides and cured. Following this, layers of dental cement were added around and above the screws, Interface, and skull to secure the Interface to the skull. Upon completion, stitches were used to gently approximate the skin (including around the arms of the Interface) while keeping the surface of the Interface exposed. The rat was monitored while waking up and for 2 hours after to ensure recovery.

Attachment: Two days after recovery, the rat was put under anesthesia to attach the Cooler. A miniscule drop of thermal paste was added between the copper contacts and the Cooler was then screwed to the Interface. A patch cable was then connected to both the Cooler and the slipring hovering above the cage on a lever arm. For studies where MRI was possible, an additional MR image was acquired at 5–7 days after implantation (with the Cooler screwed off). After this, the device was switched on, and temperature was monitored through the Arduino connected to a computer and recorded using PuTTY v0.74 (www.putty.org).

Monitoring and maintenance: The intracerebral temperatures were intermittently monitored throughout the day by connecting the computer through a local network. This enabled us to respond quickly to any sudden changes in temperature, usually due to some transient failure of the patch cable, alligator clips, or device which was rectified. Over time, there was regularly an accumulation of fur inside the heat sinks and fans. This was intermittently removed with tweezers as possible. For more complicated adjustments and corrections, the rat was put under anesthesia. Rats were given nutritionally complete diet gel regularly but were also able to eat regular food and drink water from the water bottle. Supplemental treats such as softies were also provided (Bio-Serv). Cages were cleaned once weekly. Rats were typically weighed every 2–4 days but were weighed daily if weight started falling. The procedure involved transiently disconnecting the patch cable from the slipring, moving the rat to an empty cage, and subtracting the weight of the cage, patch cable, and device.

Euthanasia: Euthanasia criteria included: 10–15% weight loss from initial weight (after recovery from Interface implantation), or signs of significant distress, porphyrin staining around the eyes, and lack of grooming and appetite. For survival studies, rats were censored if the Interface detached from the skull. When a rat reached these criteria, they were induced under 5% anesthesia and prepared for euthanasia. The patch cable and Cooler were detached. A thoracotomy was performed followed by a trans-cardial perfusion with PBS (250 mL) and then 10% formalin (250 mL). The animals were decapitated, and the skull with the brain and Interface still in place was carefully collected and left for 24 hours in 10% formalin at 4°C. Next, the Interface and skull were carefully removed, and the brain was transferred to 20% sucrose and stored at 4°C until it sunk. Subsequently, the brain was grossly sectioned, placed on an aluminum mold and buried with Optimal Cutting Temperature compound. The aluminum portion was then exposed to liquid nitrogen to initiate snap-freezing, followed by completion on dry ice. The block was stored at -80°C until further processing.

h. MRI

All MRI was performed in the Center for In Vivo Microscopy at Duke University. For images after implantation, the Cooler was unscrewed and removed from the Interface under anesthesia. Rats were positioned on a custom 3D-printed bed and eye gel and ear covers were applied. The rats were imaged in a Bruker BioSpin 7T MRI machine (Bruker, Billerica MA) with a 4-element rat brain surface coil. T1 weighted FLASH (TE/TR = 4.5/900 ms; Flip angle = 30°; 3 averages) and T2 weighted TurboRARE (TE/TR = 45/8000 ms; RARE factor of 8; 2–3 averages) axial images were acquired at a resolution of 100 µm in-plane and slice thickness of 500 µm. Contrast-enhanced T1 weighted images were acquired following a controlled injection of ProHance (Gadoteridol) via a tail vein catheter following contrast-free imaging. During all protocols, breathing was monitored via telemetry. Animal body temperature was maintained with warm air circulation in the bore of the magnet. Upon completion, if an Interface was present, the Cooler was reattached with thermal paste applied between the copper contacts. Images were analyzed on 3D Slicer v4.10.2 (www.slicer.org).

i. Histology

Brains were cryo-sectioned into 12 µm slices, collected on Superfrost+ slides, and the slides were stored at -20°C. Some slides were stained with Hematoxylin & Eosin and imaged under our microscope with a color filter. Other slides were stained with immunohistochemistry markers (from Abcam) and imaged under our microscope with fluorescent lasers. These included: mouse anti-GFP (ab1218), mouse anti-human Ku80 (ab119935), rabbit anti-rat NeuN (ab177487), rabbit anti-Ki-67 (ab16667). Secondary antibodies included: Goat anti-mouse Alexa Fluor 488 (ab150113), Goat anti-rabbit Alexa Fluor 594 (ab150080). Briefly, slides were washed with PBS and 0.5% Triton, blocked with 4% goat serum for 2 hours, followed by staining with primary antibodies diluted in 1% BSA, overnight at 4°C. The next day, slides were washed with PBS, stained with secondary antibodies diluted in 1% BSA for 2 hours, counterstained with DAPI for 15 minutes, washed and coverslipped with Fluoromount G (Southern Biotech), and left to dry overnight at room temperature. The subsequent day, nail polish was applied to the edges of the slides and then they were stored in boxes at room temperature.

j. Computational modelling

Modelling was performed on COMSOL v5.2 to study heat transfer between the probe and surrounding tissue via the finite element method. Both the steady state temperature and transient effects of initiating and stopping cooling were studied. The geometry of the model consisted of a rat brain model containing a spherical tumor and gold probe. The rat brain model, acquired from the literature [28], was generated from MRI data and smoothened to reduce anatomical indentations. The probe was modeled as a cylinder with a diameter of 1mm and height of 2.5 mm with a 45° chamfer at the tip. The tip of the probe was embedded in the tumor which was modeled as a sphere with diameters of 2 mm and 3 mm. Heat transfer was modeled with the Pennes' bioheat equation. A negative heat flux was applied to the top face of the probe to cool the probe. All other outer surfaces were fully insulated with zero heat flux.

All tissues and materials used in the model were assumed to be homogeneous and isotropic – features such as brain blood vessels were not modeled. Multiple parameters used for the tissues, perfusion, and materials were investigated (Supplementary Table 1). Original perfusion values in units of mL/100 g/min were converted into s^{-1} using a blood density of 1050 kg/m^3.

The blood perfusion and metabolic heat generation parameters were temperature-dependent based on the following equations:

$$blood\ perfusion\ =\ initial\ blood\ perfusion * 2^{(Temperature-37)/10}$$

$$metabolic\ rate\ =\ initial\ metabolic\ rate * 3^{(Temperature-37)/10}$$

Parameter	Value [units]	Source
Brain heat capacity	3630[J/(kg*K)]	[50]
Brain density	1046[kg/m^3]	[50]
Brain thermal conductivity	0.51[W/(m*K)]	[50]
Brain blood perfusion	0.018, 0.019333, 0.020333 [1/s]	[51]
Tumor multiplier	0.73, 1, 1.52, 3.96	[52]
Brain/tumor metabolic heat generation	49937[W/m^3]	[53]
Tumor heat capacity (white brain matter)	3583[J/(kg*K)]	[50]
Tumor density (white brain matter)	1041[kg/m^3]	[50]
Tumor thermal conductivity (white brain matter)	0.48[W/(m*K)]	[50]

Supplementary Table 1: Parameters used for finite-element modelling of local intracranial hypothermia.

k. Statistical analysis

All statistical analyses were performed on GraphPad Prism v9.0.2. Where appropriate, one-way, repeated measures, and two-way ANOVAs were performed with Dunnett's multiple comparisons post-hoc test unless otherwise specified. Survival was analyzed with the Log-rank Mantel-Cox test. Significance was set to 0.05 for all studies.

5. REFERENCES

1. Koshy, M. *et al.* Improved survival time trends for glioblastoma using the SEER 17 population-based registries. *J. Neurooncol.* **107**, 207–12 (2012).
2. Ostrom, Q. T. *et al.* CBTRUS Statistical Report: Primary Brain and Other Central Nervous System Tumors Diagnosed in the United States in 2012–2016. *Neuro. Oncol.* **21**, v1–v100 (2019).
3. Rapp, M. *et al.* Recurrence Pattern Analysis of Primary Glioblastoma. *World Neurosurg.* **103**, 733–740 (2017).
4. Kirkpatrick, J. P., Laack, N. N., Shih, H. A. & Gondi, V. Management of GBM: a problem of local recurrence. *Journal of Neuro-Oncology* vol. 134 487–493 (2017).
5. Brandes, A. A. *et al.* Recurrence pattern after temozolomide concomitant with and adjuvant to radiotherapy in newly diagnosed patients with glioblastoma: Correlation with MGMT promoter methylation status. *J. Clin. Oncol.* **27**, 1275–1279 (2009).
6. Weller, M. *et al.* European Association for Neuro-Oncology (EANO) guideline on the diagnosis and treatment of adult astrocytic and oligodendroglial gliomas. *The Lancet Oncology* (2017) doi:10.1016/S1470-2045(17)30194-8.
7. Gramatzki, D. *et al.* Bevacizumab may improve quality of life, but not overall survival in glioblastoma: An epidemiological study. *Ann. Oncol.* **29**, 1431–1436 (2018).
8. Kesari, S. & Ram, Z. Tumor-treating fields plus chemotherapy versus chemotherapy alone for glioblastoma at first recurrence: a post hoc analysis of the EF-14 trial. *CNS Oncol.* (2017) doi:10.2217/cns-2016-0049.
9. Jain, A. *et al.* Guiding intracortical brain tumour cells to an extracortical cytotoxic hydrogel using aligned polymeric nanofibres. *Nat. Mater.* **13**, 308–316 (2014).
10. Lyon, J. G., Carroll, S. L., Mokarram, N. & Bellamkonda, R. V. Electrotaxis of Glioblastoma and Medulloblastoma Spheroidal Aggregates. *Sci. Rep.* (2019) doi:10.1038/s41598-019-41505-6.
11. Storm, F. K. & Morton, D. L. Localized Hyperthermia in the Treatment of Cancer. *CA. Cancer J. Clin.* **33**, 44–56 (1983).
12. Cooper, I. S. & Stellar, S. Cryogenic freezing of brain tumors for excision or destruction in situ. *J. Neurosurg.* **20**, 921–930 (1963).
13. Gage, A. A., Baust, J. M. & Baust, J. G. Experimental cryosurgery investigations in vivo. *Cryobiology* **59**, 229–243 (2009).
14. Fay, T. Early experiences with local and generalized refrigeration of the human brain. *J. Neurourgery* **16**, 239–260 (1959).
15. Bohl, M. A. *et al.* The history of therapeutic hypothermia and its use in neurosurgery. *J. Neurosurg.* **130**, 1006–1020 (2019).
16. Rowbotham, G. F., Haigh, A. L. & Leslie, W. G. Cooling cannula for use in the treatment of cerebral neoplasms. *Lancet* **273**, 12–15 (1959).
17. Wion, D. Therapeutic dormancy to delay postsurgical glioma recurrence: the past, present and promise of focal hypothermia. *Journal of Neuro-Oncology* vol. 133 447–454 (2017).
18. Yang, X. F., Kennedy, B. R., Lomber, S. G., Schmidt, R. E. & Rothman, S. M. Cooling produces minimal neuropathology in neocortex and hippocampus. *Neurobiol. Dis.* **23**, 637–643 (2006).
19. Lomber, S. G., Payne, B. R. & Horel, J. A. The cryoloop: An adaptable reversible cooling deactivation method for behavioral or electrophysiological assessment of neural function. *J. Neurosci. Methods* **86**, 179–194 (1999).
20. Choi, H. A., Badjatia, N. & Mayer, S. A. Hypothermia for acute brain injury—mechanisms and practical aspects. *Nat. Rev. Neurol.* **8**, 214–222 (2012).
21. Smyth, M. D. & Rothman, S. M. Focal Cooling Devices for the Surgical Treatment of Epilepsy. *Neurosurgery Clinics of North America* vol. 22 533–546 (2011).
22. Karkar, K. M. *et al.* Focal Cooling Suppresses Spontaneous Epileptiform Activity without Changing the Cortical Motor Threshold. *Epilepsia* **43**, 932–935 (2002).
23. Kalamida, D. *et al.* Fever-range hyperthermia vs. hypothermia effect on cancer cell viability, proliferation and HSP90 expression. *PLoS One* **10**, e0116021 (2015).

24. Matijasevic, Z. Selective protection of non-cancer cells by hypothermia. *Anticancer Res.* **22**, 3267–3272 (2002).
25. Fulbert, C., Gaude, C., Sulpice, E., Chabardès, S. & Ratel, D. Moderate hypothermia inhibits both proliferation and migration of human glioblastoma cells. *J. Neurooncol.* **144**, 489–499 (2019).
26. Zhang, X. *et al.* Effect of mild hypothermia on breast cancer cells adhesion and migration. *Biosci. Trends* **6**, 313–324 (2012).
27. Kelleher, D. K., Nauth, C., Thews, O., Krueger, W. & Vaupel, P. Localized hypothermia: impact on oxygenation, microregional perfusion, metabolic and bioenergetic status of subcutaneous rat tumours. *Br. J. Cancer* **78**, 56–61 (1998).
28. Zhu, L. & Diao, C. *Theoretical simulation of temperature distribution in the brain during mild hypothermia treatment for brain injury*.
29. Plesnila, N. *et al.* Effect of hypothermia on the volume of rat glial cells. *J. Physiol.* **523 Pt 1**, 155–62 (2000).
30. Bayley, J. S. *et al.* Cold exposure causes cell death by depolarization-mediated Ca 2+ overload in a chill-susceptible insect. doi:10.1073/pnas.1813532115.
31. Salman, M. M. *et al.* Hypothermia increases aquaporin 4 (AQP4) plasma membrane abundance in human primary cortical astrocytes via a calcium/transient receptor potential vanilloid 4 (TRPV4)- and calmodulin-mediated mechanism. *Eur. J. Neurosci.* **46**, 2542–2547 (2017).
32. Ishikawa, J. *et al.* Hypothermic temperature effects on organ survival and restoration. *Sci. Rep.* **5**, 1–12 (2015).
33. Woolf, E. C., Syed, N. & Scheck, A. C. Tumor metabolism, the ketogenic diet and β-hydroxybutyrate: Novel approaches to adjuvant brain tumor therapy. *Front. Mol. Neurosci.* **9**, (2016).
34. Seyfried, T. N. & Mukherjee, P. Targeting energy metabolism in brain cancer: Review and hypothesis. *Nutrition and Metabolism* vol. 2 (2005).
35. Seyfried, T. N. *et al.* Metabolic management of brain cancer. *Biochimica et Biophysica Acta - Bioenergetics* vol. 1807 577–594 (2011).
36. Zhang, J. *et al.* The transcriptome responses of cardiomyocyte exposed to hypothermia. *Cryobiology* **72**, 244–250 (2016).
37. Zhu, V. F., Yang, J., LeBrun, D. G. & Li, M. Understanding the role of cytokines in Glioblastoma Multiforme pathogenesis. *Cancer Letters* vol. 316 139–150 (2012).
38. Nias, A. H. W., Frcr, D., Perry Mist, P. M., Photiou, A. R. & Richard, P. Modulating the oxygen tension in tumours by hypothermia and hyperbaric oxygen. *J. R. Soc. Med.* **81**, (1988).
39. Lee, S. Y. Temozolomide resistance in glioblastoma multiforme. *Genes Dis.* **3**, 198–210 (2016).
40. Gatenby, R. A., Silva, A. S., Gillies, R. J. & Frieden, B. R. Adaptive therapy. *Cancer Res.* **69**, 4894–903 (2009).
41. West, J. *et al.* Towards multidrug adaptive therapy. *Cancer Res.* **80**, 1578–1589 (2020).
42. Aronov, D. & Fee, M. S. Analyzing the dynamics of brain circuits with temperature: Design and implementation of a miniature thermoelectric device. *J. Neurosci. Methods* **197**, 32–47 (2011).
43. Cooke, D. F. *et al.* Fabrication of an inexpensive, implantable cooling device for reversible brain deactivation in animals ranging from rodents to primates. *J. Neurophysiol.* **107**, 3543–3558 (2012).
44. Imoto, H. *et al.* Use of a Peltier chip with a newly devised local brain-cooling system for neocortical seizures in the rat. Technical note. *J Neurosurg* **104**, 150–156 (2006).
45. Bakken, H. E., Kawasaki, H., Oya, H., Greenlee, J. D. W. & Howard, M. A. A device for cooling localized regions of human cerebral cortex. *J. Neurosurg.* **99**, 604–608 (2003).
46. Rockwell, S. In vivo-in vitro tumour cell lines: characteristics and limitations as models for human cancer. *Br. J. Cancer* **41**, 118–122 (1980).
47. Senapati, S., Mahanta, A. K., Kumar, S. & Maiti, P. Controlled drug delivery vehicles for cancer treatment and their performance. *Signal Transduction and Targeted Therapy* vol. 3 1–19 (2018).
48. Miller, I. *et al.* Remote control of CAR T cell therapies by thermal targeting. *bioRxiv* 2020.04.26.062703 (2020) doi:10.1101/2020.04.26.062703.
49. Riccione, K. *et al.* Generation of CAR T cells for adoptive therapy in the context of glioblastoma standard

of care. *J. Vis. Exp.* e52397 (2015) doi:10.3791/52397.

50. Hasgall, P. *et al.* IT'IS Database for thermal and electromagnetic parameters of biological tissues. itis.swiss/database (2018) doi:10.13099/VIP21000-04-0.
51. Larkin, J. R. *et al.* Quantitative blood flow measurement in rat brain with multiphase arterial spin labelling magnetic resonance imaging. *J. Cereb. Blood Flow Metab.* **39**, 1557–1569 (2019).
52. Boxerman, J. L., Schmainda, K. M. & Weisskoff, R. M. *Relative Cerebral Blood Volume Maps Corrected for Contrast Agent Extravasation Significantly Correlate with Glioma Tumor Grade, Whereas Uncorrected Maps Do Not*. www.ajnr.org.
53. Wang, Y., Zhu, L. & Rosengart, A. J. Targeted brain hypothermia induced by an interstitial cooling device in the rat neck: Experimental study and model validation. *Int. J. Heat Mass Transf.* **51**, 5662–5670 (2008).